Lead Article

Acta Cryst. (1993). A**49**, 231–260

On the Accurate Measurement of Structure-Factor Amplitudes and Phases by Electron Diffraction*

By J. C. H. Spence

Department of Physics, Arizona State University, Tempe, AZ 85287, *USA*

(*Received* 27 *January* 1992; *accepted* 20 *August* 1992)

Abstract

A review is given of research into the measurement of crystal structure-factor amplitudes and phases by transmission electron diffraction. Accuracies for amplitudes are commonly a fraction of a percent (after conversion to X-ray structure factors) while phases may now be measured in favorable cases using three-beam electron diffraction to an accuracy of much better than 1°. Following a brief review of theory, the main techniques are outlined. These include quantitative convergent-beam electron diffraction, the critical-voltage method, the intersecting Kikuchi- and HOLZ-line methods and methods based on weak high-order reflections in wide-angle patterns. Enantiomorphs and polarity are discussed. Summaries are given of measurements of the mean inner potential and of structure factors generally. A brief review of the implications of this work for studies of crystal bonding and ordering in alloys is given, and its use to test *ab initio* computations of charge density. The mean inner potential is found to be the quantity most sensitive to the bonding distribution of valence electrons and sensitively constrains accurate X-ray structure-factor measurements. Electron diffraction techniques are to be preferred for studies of individual microcrystals or artificially formed structures and for the very accurate measurement of structure-factor phases in acentric crystals with small unit cells.

1. Introduction

The development of synchrotron sources for X-ray diffraction and of powder diffraction methods for neutrons, together with the remarkable computing power of new small computers and their sophisticated crystallographic software, might appear to give the modern crystallographer all the tools required for the study of organic and inorganic crystals. The need for an additional 'electron crystallography' is not immediately apparent. However, each probe of the solid state interacts differently with matter and thus exposes a different aspect of a crystal. In addition, electron beams (unlike X-rays and neutrons) may be focused down to a probe of sub-nanometer dimensions using electron lenses, allowing microphases which cannot easily be crystallized to be studied. Very briefly (and neglecting second-order effects), while X-ray methods give us information on the ground-state crystal charge density and neutrons on magnetic properties, lattice vibrations and crystal structure, electrons probe the electrostatic crystal potential and internal magnetic fields. We shall see that the interaction of a focused kV electron beam with a thin crystal is unique in its ability to provide highly accurate measurements of low-order structure-factor amplitudes and phases from extremely small sample volumes. This enhanced accuracy is a consequence of the way in which Poisson's equation relates X-ray and electron structure factors. For the benefit of readers with a background in X-ray diffraction, it should be said that electron diffraction techniques measure the Fourier coefficients V_g (in V) of the total ground-state crystal potential (including the nuclear contribution) and we shall refer to these V_g loosely in this article as structure factors. They are related to X-ray structure factors (the Fourier coefficients of the crystal charge density, excluding the nuclear contribution) by Poisson's equation if high-energy electrons are used. (At beam energies below a few kV, exchange and virtual inelastic corrections to the potential mean that Poisson's equation and the Mott–Bethe formula cannot be used.) For non-centrosymmetric (acentric) crystals, measurements of X-ray structure-factor phases may now be made by electron diffraction with an unrivalled accuracy of a fraction of a degree for small-unit-cell inorganic crystals. As discussed in § 5, these measurements allow, amongst other things, the study of crystal bonding and of short-range order and composition in alloys, in addition to providing measurements of Debye temperatures. They may also be used to test band-structure calculations. Problems of defects, dispersion and extinction are avoided, or are accounted for exactly in the data analysis. The electron microdiffraction method used may thus be applied to the

* *Editorial note*: This invited paper is one of a series of comprehensive Lead Articles which the Editors invite from time to time on subjects considered to be timely for such treatment.

0108-7673/93/020231-30$06.00 © 1993 International Union of Crystallography

great variety of metastable microphases which occur in minerals (or in modern synthesized composite materials) and to those artificial multilayer or quantum-well structures which could not readily be studied by other techniques. The real power of electron-beam methods now lies in their accuracy and ability to study real materials rather than synthetically grown single-crystal analogs.

Experimental and other considerations also influence our choice of probes, such as particle lifetime, the brightness of available sources, the efficiency of detectors, the strength of the scattering and the size of the sample volume irradiated. Factors favoring the use of electron diffraction include the high brightness of field-emission electron sources (comparable to that of synchrotrons), the high detective quantum efficiency of electron detectors (which approaches unity) and the strong scattering cross sections involved.

In the general context of the field of electron microscopy, the measurement of dynamical diffraction intensities discussed in this review constitutes a small and highly specialized field of research - the overwhelming bulk of the work in electron microscopy is concerned with imaging or microanalysis and with the analysis of diffraction-pattern symmetries and geometries rather than their intensities. Thus the identification of a microphase from a list of candidate structures is usually based on evidence from the characteristic X-ray spectra and from the symmetry of the microdiffraction patterns. The ability of modern electron microscopes to form images of crystals at atomic resolution has proven invaluable for the study of crystal defects and the atomic mechanisms involved in phase transformations. The magnetic interaction also provides a uniquely powerful ability to study the spatial distribution of magnetic fields in ferromagnets and superconductors by electron holography. These imaging and microanalytical techniques account for most of the impact of electron microscopy on materials physics and chemistry. The development of truly quantitative methods in electron crystallography is a more recent development, made possible by advances in electron spectrometer design, field emission guns and computer hardware and software. Recent work suggests that the electron microdiffraction pattern is now the most accurately quantifiable signal obtainable from a modern electron microscope. With the appearance of commercial imaging energy filters, convenient field-emission guns and the new workstations, we therefore anticipate considerable growth in this field.

Historically, the early workers were deterred from using electron beams for crystallography by the apparent intractability of the multiple-scattering problem, first formulated by H. Bethe for the reflection case (Bethe, 1928). Structure-factor measurements were nevertheless attempted at an early stage, however, using two-beam theory (Blackman, 1939; MacGillavry, 1940) applied to the first experimental convergent-beam electron diffraction (CBED) patterns. These patterns, not greatly different from modern patterns, were obtained from mica as early as 1939 (Mollenstedt, 1989). Considerable effort was also then devoted to exploring the limits of the kinematic approximation (Vainshtein, 1964). Much of the early work was therefore applied to crystals containing light elements [including hydrogen (Cowley, 1953)], such as organic films, paraffin wax, monohydrates of halides *etc.*, and was based on single-scattering theory applied to polycrystalline material. Slow but steady progress has been made in the analysis of extremely thin single-crystal organic films using a combination of imaging and diffraction methods based on single-scattering theory (Dorset, 1983; Unwin & Henderson, 1975). (By indicating atomic positions directly, the associated imaging thus 'solves' the phase problem of X-ray crystallography.) In favorable cases where thin organic films crystallize, these structures have now been solved in three dimensions to a resolution of a few Å. This work, which has also come to be known as electron crystallography, is not covered in this review because the techniques and data analysis used have little in common with work on inorganic crystals. [Emphasis falls on the important problems of sample preparation, radiation damage and bending (Dorset, 1983) for organic films, rather than on questions of multiple scattering and accuracy.] For inorganic crystals, the kinematic theory was found to fail for even a few atomic layers of medium-atomic-weight material at 100 kV. Reviews of this early work can be found in Pinsker (1949), Vainshtein (1964) and Cowley (1967). Early work on clay minerals is reviewed in Zvyagin (1967). With the availability of inexpensive reduced-instruction-set computer (RISC) workstations, it has become possible to perform dynamical computations involving many hundreds of interacting beams in a few minutes so that multiple-scattering effects are now routinely incorporated exactly and indeed may be used to advantage (for example to expose structure-factor phases), as forseen by the early researchers (Kambe, 1957). The development of nanoprobe instruments has removed the need to work with polycrystalline material in which the degree of orientational disorder was always uncertain.

This review aims to summarize most of the literature on the measurement of structure-factor amplitudes and phases by electron diffraction and the theoretical and experimental principles on which the measurements are based. The material can be organized by technique or by material - I have attempted to do both in §§ 3 and 5. Experimental aspects are included in § 3. Two recent books contain review chapters on this topic (Cowley, 1992; Spence & Zuo, 1992) and Vol. 41, No. 3 of the *Australian*

Journal of Physics is devoted to accuracy in structure-factor measurement generally. We shall see that, although no fundamental reason prevents it, few unknown crystal structures have been solved using electron diffraction data alone. The bulk of the review is therefore concerned with the problem of refining structure factors for small-unit-cell crystals of known structure. Three main techniques have been used for this purpose - the critical-voltage method, the intersecting Kikuchi [or higher-order Laue zone (HOLZ)] line method and the quantitative convergent-beam (CBED) technique. The following abreviations are therefore used frequently: higher-order Laue zone (HOLZ), intersecting Kikuchi-line method (IKL) (similar to the Renninger effect in X-ray diffraction), zero-order Laue zone (ZOLZ) and critical voltage (CV). In the light of past misunderstandings with the X-ray community, it is important to point out that we define a HOLZ as any plane of reciprocal-lattice points which does not pass through the origin. (Often this plane will lie normal to the incident electron beam.) The ZOLZ includes the origin. These various techniques are discussed in § 3 (with emphasis on novel techniques for phase measurement) following a brief review of the relationship between the different interactions involved in X-ray and electron crystallography. § 5 discusses the special case of the zero-order Fourier coefficient V_0 of the crystal electrostatic potential, which provides a sensitive characterization of the distribution of bonding electrons. (The corresponding quantity in X-ray crystallography, the zero-order coefficient of charge density, is equal to the number of electrons in the unit cell.) § 6 lists many electron diffraction measurements by material. § 7 summarizes what we have learnt from these measurements about materials and suggests future directions.

2. Theory. What is measured. Temperature effects. Absorption

We first discuss the relationship between the intensities in electron diffraction patterns and the crystal potential, its charge density and certain contributions to the crystal total energy.

Whereas X-ray crystallography is based on Maxwell's equations (Zachariasen, 1932) (or quantum electrodynamics), electron diffraction commences with the Schroedinger (or Dirac) equation. These are related through the many-electron wavefunction for the crystal electrons, which defines both the crystal charge density and electrostatic potential. We now outline the relationship between the quantities measured in electron and X-ray diffraction from first principles. For the system of the beam electron (with interaction Hamiltonian H_b and total energy E_b) traversing a thin crystal (with Hamiltonian H_c and total energy E_{cr}), the Schroedinger equation becomes, in SI units,

$$[-(h^2/8\pi^2m)\nabla^2+H_c+H_b]\Psi=(E_b+E_{cr})\Psi \quad (1)$$

where

$$H_c=-\sum_{i=1}^{ZN}(h^2/8\pi^2m)\nabla_i^2-\sum_{i=1}^{ZN}\sum_{a=1}^{N}Ze^2/4\pi\varepsilon_0|R_a-r_i|$$
$$+\tfrac{1}{2}\sum_{i\neq j}^{ZN}\sum^{ZN}e^2/4\pi\varepsilon_0r_{ij}+\tfrac{1}{2}\sum_{a\neq b}^{N}\sum^{N}Z^2e^2/4\pi\varepsilon_0|R_{ab}| \quad (2)$$

for a crystal containing N identical atoms, each of Z electrons. We have ignored inelastic electron scattering. Here $r_{ij}=|\mathbf{r}_i-\mathbf{r}_j|$ are crystal electron coordinates, while $R_{ab}=|\mathbf{R}_a-\mathbf{R}_b|$ are nuclear coordinates. If the electron-beam coordinate is $\mathbf{r}$, then

$$H_b=\sum_j e^2/4\pi\varepsilon_0|\mathbf{r}-\mathbf{r}_j|-\sum_a Ze^2/4\pi\varepsilon_0|\mathbf{r}-\mathbf{R}_a|. \quad (3)$$

It has been shown (Rez, 1978) that the exchange energy between the beam and crystal electrons is negligible. Thus, because of its high energy, the beam electron can be distinguished from the crystal electrons. If the total wavefunction is then written in the absence of absorption as a single product of wavefunctions, we have

$$\Psi(\mathbf{r},\mathbf{r}_1,\mathbf{r}_2,\ldots,\mathbf{r}_n)=\psi_c(\mathbf{r}_1,\mathbf{r}_2,\ldots,\mathbf{r}_n)\psi_b(\mathbf{r}). \quad (4)$$

Here ψ_c is an antisymmetric linear combination of one-electron wavefunctions.

For the crystal electrons,

$$H_c\psi_c=E_{cr}\psi_c. \quad (5)$$

From these equations, it can be shown that, if absorption is neglected, the beam electron wavefunction alone now satisfies a Schroedinger equation

$$(1/4\pi^2)\nabla^2\psi_b+(2m/h^2)(\textstyle\int\psi_c^*H_b\psi_c\,d\tau)\psi_b=K^2\psi_b \quad (6)$$

where $K^2=(2m/h^2)E_b$ is the beam electron wave vector in free space. Thus, $V(\mathbf{r})$, the potential seen by the beam electron, whose structure factors V_g we may measure in an electron diffraction experiment, is the matrix element in the above equation (divided by e). It may be solved using Bloch waves and using a Fourier expansion for $V(\mathbf{r})$, as described in texts on electron diffraction (Hirsch, Howie, Nicholson, Pashley & Whelan, 1977; Reimer, 1984).

If ψ_c is now written as a Slater determinant in terms of one-electron wavefunctions $\varphi_j(\mathbf{r}_j)\alpha_j$ (with spin part α_j), then (Raimes, 1961)

$$eV(\mathbf{r})=\int\psi_c^*H_b\psi_c\,d\tau$$
$$=\sum_j\int\frac{e^2|\varphi_j(\mathbf{r}')|^2}{4\pi\varepsilon_0|\mathbf{r}-\mathbf{r}'|}d\mathbf{r}'-\sum_i\frac{Ze^2}{4\pi\varepsilon_0|\mathbf{r}-\mathbf{R}_i|} \quad (7)$$
$$=e\int\frac{e\rho(\mathbf{r}')}{4\pi\varepsilon_0|\mathbf{r}-\mathbf{r}'|}d\mathbf{r}'-\sum_i\frac{Ze^2}{4\pi\varepsilon_0|\mathbf{r}-\mathbf{R}_i|}. \quad (8)$$

This equation has the form of the integral solution of Poisson's equation and expresses $V(\mathbf{r})$, the potential seen by the beam electron, as the sum of the potential due to a (dimensionless) electronic charge $\rho(\mathbf{r}) = \psi_c\psi_c^* = \sum_j |\varphi_j(\mathbf{r})|^2$ and a nuclear potential. This defines $\rho(\mathbf{r})$, as obtainable by electron or X-ray diffraction studies, in terms of the many-electron crystal wavefunction ψ_c. The total crystal ground-state energy is, in an obvious notation,

$$E_{\rm cr} = \int \psi_c^* H_c \psi_c \,{\rm d}\tau \qquad (9)$$

$$= E_{\rm kin} + E_{\rm e/nuc} + E_{\rm e/e} + E_{\rm nuc/nuc} + E_{\rm ex} \qquad (10)$$

where

$$E_{\rm e/e} = \frac{1}{2}\int\int \frac{e^2\rho(\mathbf{r}_j)\rho(\mathbf{r}_j)}{4\pi\varepsilon_0|\mathbf{r}_i - \mathbf{r}_j|}\,{\rm d}\mathbf{r}_j\,{\rm d}\mathbf{r}_i = E_H \qquad (11)$$

using the same determinant of one-electron wavefunctions. Thus, as in X-ray crystallography, the energy contribution to the crystal total energy which might be measured by electron diffraction is the electrostatic, Coulomb or Hartree energy E_H. The kinetic energy of the crystal electrons $E_{\rm kin}$ is related (under certain conditions) to their potential energy through the virial theorem, while the nuclear interaction term $E_{\rm nuc/nuc}$ may be evaluated by an Ewald lattice sum. Thus it is the exchange and correlation energy $E_{\rm ex}$ which is not accessible in electron diffraction experiments, since this depends in a complicated way on cross terms between the complex one-electron crystal electron wavefunctions $\varphi(\mathbf{r}_j)$. It has, however, been shown to be a unique universal functional of $\rho(\mathbf{r})$ (Hohenberg & Kohn, 1964).

The electrostatic energy E_H may be expressed in terms of X-ray structure factors $f(s)$. For example, for a diatomic molecule it is proportional to (Spackman & Maslen, 1986)

$$E_H = \int_n^\infty [Z_a - f_a(\mathbf{S})][Z_b - f_b(\mathbf{s})]J_0(\mathbf{sR})\,{\rm d}s. \qquad (12)$$

The magnitude of the missing term $E_{\rm ex}$ depends on the material, however. For diamond, for example, $E_{\rm ex} = 2$ eV (Chadi, 1989). We conclude that $E_{\rm ex}$ cannot be neglected and that $E_{\rm cr}$ cannot easily be determined from electron diffraction data.

It has also been shown that the corrections to $V(\mathbf{r})$, the potential seen by the beam electron, due to virtual inelastic scattering are negligible (Smart & Humphreys, 1978; Rez, 1978).

The Fourier coefficients of $V(\mathbf{r})$ (in V) are the electron structure factors $V_{\mathbf{g}}$ measured by electron diffraction. Since we have adopted the sign convention used in most of the electron diffraction and solid-state-physics literature [in which a plane wave is taken to have the form $\exp(+2\pi i\mathbf{K}\cdot\mathbf{r})$], our expressions for electron structure factors have the opposite signs from those used in *International Tables for Crystallography* (1989) and in X-ray work generally. [A review article using the crystallographic convention can be found in Spence (1992).] The effect of a sign change is to conjugate all structure factors in acentric crystals and must be taken into account when comparing X-ray and electron phase determinations. Thus,

$$V(\mathbf{r}) = \sum_g V_g \exp(+2\pi i\mathbf{g}\cdot\mathbf{r}). \qquad (13)$$

These coefficients $V_{\mathbf{g}}$ may now be related to the dimensionless Fourier coefficients $F^x(\mathbf{g})/\Omega$ of $\rho(r)$ which are measured by X-ray diffraction, since the Fourier transform of (8) gives the famous Mott–Bethe relationship (in SI units)

$$V_{\mathbf{g}} = (|e|/16\pi^2\varepsilon_0\Omega)\sum_i\{[Z_i - f_i^x(s)]/s^2\}$$
$$\times\exp(-B_is^2)\exp(-2\pi i\mathbf{g}\cdot\mathbf{r})$$
$$= (h^2/8\pi\varepsilon_0 m_e|e|\Omega)F_{\mathbf{g}}^B. \qquad (14)$$

Here the sum is over the unit cell of volume Ω (m^3) and $F_{\mathbf{g}}^B$ is the electron structure factor according to the old (Born-approximation) system (*International Tables for Crystallography* before 1990). $V_{\mathbf{g}}$ is given in V, m_e is the rest mass of the electron and $s = \sin\theta_B/\lambda = |\mathbf{g}|/2$. The Debye-Waller factor is $B_i = 8\pi^2\langle u^2\rangle$ for species i, with $\langle u^2\rangle$ the mean-square vibrational amplitude of the atom. If B, s and Ω are instead given in Å units, then $V_{\mathbf{g}}$ is given in V as

$$V_{\mathbf{g}} = (1.145896/\Omega)\sum_i\{[Z_i - f_i^x(s)]/s^2\}$$
$$\times\exp(-B_is^2)\exp(-2\pi i\mathbf{g}\cdot\mathbf{r}_i)$$
$$= (47.878009/\Omega)F_{\mathbf{g}}^B. \qquad (15)$$

Two other quantities commonly used in the literature are the beam-energy-dependent electron structure factor $U_{\mathbf{g}}$ and the two-beam extinction distance ξ_g,

$$U_{\mathbf{g}} = \gamma F_{\mathbf{g}}^B/\pi\Omega = 2m|e|V_{\mathbf{g}}/h^2 \qquad (16)$$

$$\xi_{\mathbf{g}} = 1/(\lambda|U_{\mathbf{g}}|) = \pi/(|V_{\mathbf{g}}|\sigma) = \pi\Omega/(\gamma\lambda|F_{\mathbf{g}}^B|) \qquad (17)$$

where γ is the relativistic constant. For $V_{\mathbf{g}}$ in V and $U_{\mathbf{g}}$ in Å^{-2}, we then have

$$U_{\mathbf{g}} = 0.006648352(1 + 1.956934\times10^{-6}E_0)V_{\mathbf{g}}. \qquad (18)$$

If the X-ray structure factor is defined (with unconventional signs) by

$$F_{\mathbf{g}}^x = \sum_i f_i^x(s)\exp(-B_is^2)\exp(-2\pi i\mathbf{g}\cdot\mathbf{r}), \qquad (19)$$

where the electronic charge density (in electrons per cell) is

$$\rho(\mathbf{r}) = \Omega^{-1}\sum_g F_{\mathbf{g}}^x\exp(2\pi i\mathbf{g}\cdot\mathbf{r}), \qquad (20)$$

then we obtain the following expression for the retrieval of an X-ray structure factor $F_{\mathbf{g}}^x$ from electron

diffraction data:

$$F_{\mathbf{g}}^{x} = \sum_i Z_i \exp(-B_i s^2) \exp(-2\pi i \mathbf{g} \cdot \mathbf{r}) - (8\pi^2 \varepsilon_0 h^2 \Omega s^2 / \gamma m_e e^2) U_{\mathbf{g}} \quad (21)$$

$$= \sum_i Z_i \exp(-B_i s^2) \exp(-2\pi i \mathbf{g} \cdot \mathbf{r}) - (C \Omega s^2 / \gamma) U_{\mathbf{g}}. \quad (22)$$

Here the numerical constant $C = 131.2625$ if s, Ω and $U_{\mathbf{g}}$ are given in Å units.

The role of the temperature factor in conversions between X-ray and electron structure factors is important. The atomic vibrational amplitude u is appreciable even at 0 K, where in some materials it falls to only about half its room-temperature value. Thus, the observable crystal potential is a temperature-dependent quantity – the static potential computed from band-structure calculations is not an experimental observable. We see that a knowledge of the Debye–Waller factor B_i is essential in order to convert a structure factor $U_{\mathbf{g}}$ measured by electron diffraction at temperature T into the corresponding X-ray structure factor $F_{\mathbf{g}}^{x}$ at temperature T. A knowledge of B_i is similarly required to convert measured X-ray scattering factors into electron scattering factors for the same temperature.

Relatively little attention has been devoted to the problem of measuring temperature factors by electron diffraction. The most complete recent studies have been those of Kuroda, Tomokiyo & Eguchi (1981), Matsuhata, Tomokiyo, Kuroda & Eguchi (1983) and Matsumura, Tomokiyo & Oki (1989). An analysis of the effects of temperature on extinction distances in electron diffraction is given by Howie & Valdre (1967). Here it is shown that the temperature dependence of electron structure factors for an isotopic centric crystal containing only one type of atom can be written as

$$U_{\mathbf{g}}(\text{tot.}) = U_{\mathbf{g}} \exp(-B\mathbf{g}^2/4) + iU'_{\mathbf{g}}(\text{phonon})$$

where $B = B(T)$ is the temperature factor and $U'_{\mathbf{g}}$ is the contribution to the imaginary part of the optical potential used to describe phonon scattering, commonly referred to as 'absorption'. Anharmonic vibrations will further modify the real part of $U_{\mathbf{g}}$. For atoms vibrating independently in an anharmonic potential, it may be shown (Willis & Pryor, 1975) that structure factors may be written

$$V_g = \Omega^{-1} \sum_j f_j^e(s) T_j(s) \exp(-2\pi i \mathbf{g} \cdot \mathbf{r}_j)$$

where, in general, both $f(s)$ and $T(s)$ are now complex. Anharmonic vibrations introduce both an imaginary part to $T(s)$ and a correction to the real (harmonic) part of $T(s)$.

By measuring the intensity of several reflections (particularly high orders) as a function of $\mathbf{g}$, it is possible to measure $B(T)$ using electron diffraction data. Measurements may also be made at several temperatures. In one case, for example (Goodman, 1971), values of both $U'_{\mathbf{g}}$ and B were determined separately for MgO. In such a centric crystal, the Debye–Waller factor affects the real (elastic) potential (and therefore the ratio A/B in Fig. 2, to be discussed in more detail below) and, most sensitively, the intensity of the high-order reflections. We will see that the effects of absorption for beam $\mathbf{g}$ are best measured from the asymmetry of the zero-order disc with $\mathbf{g}$ at the Bragg condition. [The zero-order disc provides the rocking curve for the 'direct' ($\mathbf{g} = 0$) beam.] The two effects may therefore be separated readily in centric crystals. The influence of the bonding effect may be disentangled from the temperature effect by matching reflections as a function of $\mathbf{g}$, high-order reflections being more sensitive to the latter and low orders to the former. Both the critical-voltage effect and the intersecting HOLZ (or Kikuchi-line) method to be discussed have also been used to measure Debye–Waller factors. These depend sensitively on temperature, since the IKL gap and the critical voltage both depend on the real part of the structure factor in centric crystals. Thus, temperature may be used as an adjustable parameter to fine-tune patterns near the critical voltage (Sellar, Imeson & Humphreys, 1980). In recent work, both critical voltages and Kikuchi-line splittings for Si, Ge, Al, Cu and Fe have all been measured as a function of temperature (Matsumura, Tomokiyo & Oki, 1989). These workers find that the anharmonic contribution to the temperature factor in the metals is readily detectable above 300 K, but is very small for the semiconductors. They derive values of structure factors in good agreement with those obtained by X-ray and neutron diffraction. There would appear to be considerable scope for more studies of this type, provided that adequate CBED facilities and energy filtering can be fitted to high- and medium-voltage electron microscopes. The use of HOLZ lines in CBED patterns to measure thermal expansion coefficients is described by Angelini & Bentley (1984).

From (15) we see that, at small scattering angles, small changes in f^x result in large changes in f_i^e. Thus, if f_i^e is known to a particular percentage error, f^x may be deduced to a greater accuracy. This observation has been the basis for much of the interest in quantitative electron crystallography, including the possibility of detecting hydrogen in crystals.

The asymptotic behavior of the electron scattering factors for large and small values of s is considered by Peng & Cowley (1988). At large angles the angular dependence of Rutherford scattering is required. New relativistic Hartree-Fock (RHF) calculations more accurate than those in *International Tables for Crystallography* at high angles have recently been published by Fox, O'Keefe & Tabbernor (1989). The zero-angle

value is discussed in § 5, where it is related to the diamagnetic susceptibility.

The Bloch-wave dynamical theory of high-energy transmission electron diffraction (HEED) has been described in many texts and review articles - in this review we will use the symbols, derivations and results given by Spence & Zuo (1992) and quote only the main results. This formalism is also consistent with that of Humphreys (1979), to which review the reader is referred for background. Students new to the field looking for pedagogically sound reviews are also particularly referred to Hirsch *et al* (1977), Metherell (1975) and Reimer (1984). Very briefly, (6) must be rederived in a relativistically correct form and (13) used, together with a Bloch-wave expansion of the total beam electron wavefunction. We define $g_n = \mathbf{g} \cdot \mathbf{n}$ and $K_n = \mathbf{K} \cdot \mathbf{n}$, where $\mathbf{n}$ is a unit vector normal to a thin slab of crystal traversed by the beam. This leads to (Lewis, Villagrana & Metherell, 1978; Spence & Zuo, 1992)

$$2\mathbf{K}S_\mathbf{g}C_\mathbf{g}^{(j)} + \sum_\mathbf{h} U_{\mathbf{g}-\mathbf{h}}C_\mathbf{h}^{(j)} = 2K_n(1+g_n/K_n)\gamma^{(j)}C_\mathbf{g} \quad (23)$$

where γ and $C_\mathbf{g}$ are eigenvalues and eigenvectors to be determined by computation and $S_\mathbf{g}$ is the excitation error for beam $\mathbf{g}$. This equation includes all HOLZ effects, boundary inclination effects and absorption terms and may be applied to acentric crystals. The most important approximations have been the neglect of backscattering, exchange effects between beam and crystal electrons and virtual inelastic scattering. To transform this equation into a linear eigenvalue equation, we define new eigenvector elements

$$B_\mathbf{g}^{(j)} = (1+g_n/K_n)^{1/2}C_\mathbf{g}^{(j)} \quad (24)$$

so that, using (23),

$$\begin{aligned} &2\mathbf{K}S_\mathbf{g}B_\mathbf{g}^{(j)}/(1+g_n/K_n) \\ &\quad + \sum_\mathbf{h} B_\mathbf{h}^{(j)}U_{\mathbf{g}-\mathbf{h}}/[(1+g_n/K_n)^{1/2}(1+h_n/K_n)^{1/2}] \\ &\quad = 2K_n\gamma^{(j)}B_\mathbf{g}^{(j)}. \end{aligned} \quad (25)$$

This is the fundamental eigenvalue equation to be solved in order to describe coherent multiple electron scattering in a thin slab of crystal. If the surface normal is approximately antiparallel to the beam, so that $K_n \gg g_n$, then g_n/K_n is negligible and we have

$$2\mathbf{K}S_\mathbf{g}C_\mathbf{g}^{(j)} + \sum_\mathbf{h} U_{\mathbf{g}-\mathbf{h}}C_\mathbf{h}^{(j)} = 2K_n\gamma^{(j)}C_\mathbf{g}.$$

This equation may be written in matrix form

$$\mathbf{A}\mathbf{C}^i = 2K_n\gamma^j\mathbf{C}^i \quad (26)$$

where the off-diagonal entries of the 'structure matrix' $\mathbf{A}$ are $U_{\mathbf{g}-\mathbf{h}}$, while the diagonal entries are the excitation error terms $2KS_\mathbf{g}$. Here $\mathbf{C}^j$ is a column vector. Equation (26) includes HOLZ effects in an approximate way and the crystal tilt through the term in K_n. The distances γ^i have a geometric interpretation as the displacement, in the direction of the surface normal, of the true dynamical dispersion surface from spheres drawn about every reciprocal-lattice point. These spheres have radii $\mathbf{K}$. [For diagrams of the relevant dynamical dispersion surfaces, see Hirsch *et al.* (1977), Metherell (1975) and Spence & Zuo (1992).]

For centrosymmetric crystals without absorption, $\mathbf{A}$ is real, symmetric and Hermitian. For centrosymmetric crystals with absorption, $\mathbf{A}$ is complex, symmetric and not Hermitian.

If n beams are included, the structure matrix $\mathbf{A}$ has dimensions $n \times n$ and (26) gives n eigenvalues and n eigenvectors. These define the wavefield inside the crystal which may be written according to the 'Darwin representation' (Hirsch *et al.*, 1977) of n plane waves propagating in the crystal, each in the direction of $\mathbf{K}+\mathbf{g}$. Thus,

$$\Psi(\mathbf{r}) = \sum_\mathbf{g} \varphi_\mathbf{g} \exp[2\pi i(\mathbf{K}+\mathbf{g})\cdot\mathbf{r}]. \quad (27)$$

Then the wave amplitude at crystal thickness t becomes

$$\varphi_g(t) = \sum_{i=1}^{n} c_i C_\mathbf{g}^i \exp(2\pi i\gamma^i t). \quad (28)$$

Although the Bloch waves in the ZOLZ contributing to a particular Bragg beam travel in slightly different directions inside the crystal, for a parallel-sided slab of perfect crystal they are focused to the same point at the detector outside the crystal because they all have the same x and y wave-vector components. The excitation coefficients c_i are to be determined by matching the incident waves onto waves inside the crystal at the entrance surface. That is, we set $t=0$ in (28) and then solve the resulting linear equation for c_i. The wavefield inside crystal is then found to be

$$\begin{pmatrix} \varphi_0(t) \\ \varphi_\mathbf{g}(t) \\ \vdots \end{pmatrix} = C \begin{pmatrix} \exp(2\pi i\gamma^1 t) & \dots & 0 \\ \vdots & & \vdots \\ 0 & \dots & \exp(2\pi i\gamma^n t) \end{pmatrix} \times C^{-1} \begin{pmatrix} \varphi_0(0) \\ \varphi_\mathbf{g}(0) \\ \vdots \end{pmatrix}. \quad (29)$$

The matrix $\mathbf{S} = \mathbf{C}\{\exp(2\pi i\gamma t)\}\mathbf{C}^{-1}$ is known as the 'scattering matrix' and relates the incident waves to the scattered waves for a crystal of thickness t.

If absorption is not included, the inverse of the eigenvector matrix is the transposed conjugate of the eigenvector matrix, *i.e.* $C^{-1} = C^\dagger$. For a single incident plane wave [$\varphi_0(0) = 1$ and $\varphi_\mathbf{g}(0) = 0$], we find $c_i = C_0^{i*}$ without absorption and $c_i = C_0^{i-1}$ with absorption. The C_0^{i-1} are the elements of the first column of the inverse of the matrix whose elements are $C_\mathbf{g}^i$ (column i, row $\mathbf{g}$). The intensity of a particular Bragg beam (for a

given incident plane wave **K**) is then found using

$$I_{\mathbf{g}}(K_x, K_y) = |\varphi_{\mathbf{g}}(t)|^2 = \left|\sum_{i=1}^{n} C_0^{i-1} C_{\mathbf{g}}^i \exp(2\pi i \gamma^i t)\right|^2 \quad (30)$$

where t is again the crystal thickness. A Fortran listing of a computer program which evaluates (25) and (30) can be found in Zuo, Gjønnes & Spence (1989).

Dynamical intensities may also be computed by the multislice method, which has important advantages for defects, where the method of periodic continuation must be used, and for very small (subnanometer) coherent electron probes. For accurate structure-factor refinement in perfect crystals, however, it is usually necessary to include all appreciable HOLZ interactions. The multislice method then becomes inefficient (particularly if the crystal period in the beam direction is large) since it includes all lattice points in the three-dimensional reciprocal lattice, rather than just those required near the Ewald sphere, as in the Bloch-wave method. Yet the speed of modern workstations is now so great, particularly if combined with array-processor hardware for the Fourier series needed by the multislice algorithm, that the two methods may be competitive in many cases. An important advantage of the multislice method is that, if the slice thickness is chosen correctly (Anstis, 1990), the computation is not self-normalizing, as for the Bloch-wave method. Thus, from the sum of intensities in a multislice, it is possible to determine whether sufficient beams have been included. This information is not present in Bloch-wave calculations. For a fuller discussion and a comparison of these numerical methods, see Kilaas, O'Keefe & Krishnan (1987), Spence & Zuo (1992) and Krakow & O'Keefe (1989).

We now consider the effects of inelastic scattering on structure-factor refinement. This may be accounted for in the theory by the introduction of an optical potential (Yoshioka & Kainuma, 1962) $V(\mathbf{r}) = V^c(\mathbf{r}) + iV'(\mathbf{r})$, with $V^c(\mathbf{r})$ the real crystal potential (describing the interaction of the incident electron with the crystal electrons and the nuclei) and $V'(\mathbf{r})$ a second real potential which accounts for depletion of the elastic wavefield by inelastic scattering. Because virtual inelastic scattering and exchange corrections can be neglected at kV energies, $V_c(\mathbf{r})$ (the Coulomb or Hartree electrostatic potential) can be related to the true ground-state charge density using Poisson's equation. If an ideal energy filter is used which excludes all inelastic scattering from a CBED pattern, then there are two main experimental effects of absorption. Firstly, under idealized two-beam conditions, an asymmetry is introduced into the zero-order disc around the Bragg condition and, secondly, differences arise between the intensities of the **g** and $-\mathbf{g}$ discs at the Bragg condition in noncentrosymmetric crystals. [This has corresponding effects on energy-loss spectra (Taftø, 1987).] For high-energy electrons, there are three important inelastic scattering mechanisms: (1) inelastic scattering resulting from the excitation of crystal electrons; (2) excitation of plasmons; (3) excitation of phonons. The plasmon scattering contributes to the mean absorption (V_0') only and the contributions of electron scattering decrease rapidly as the scattering angle increases. The contribution to $V_{\mathbf{g}}'(\mathbf{g} \neq 0)$ comes mostly from phonon scattering (Hall & Hirsch, 1965; Radi, 1970; Yoshioka & Kainuma, 1962). The mean absorption describes an overall attenuation of the incident electrons. Absorption coefficients have been calculated in the past for a number of crystals by several authors [see Reimer (1984) for a review]. A parametric fit for the absorption coefficients [such as $V_{\mathbf{g}}'/V_{\mathbf{g}} = (A + Bg)g$] has also been proposed (Ichimiya, 1985) and values of A and B have been given for some crystals (Voss, Lehmpfuhl & Smith, 1980). Calculations for phonon absorption based on the Einstein model, using the Debye–Waller factor as input, appear to be useful as a first approximation and as a basis for further refinement. The Debye–Waller factor is taken from experimental X-ray or neutron diffraction results or from theoretical calculations. Calculations for total absorption coefficients, including plasmon excitation, single-electron excitation and phonon scattering, are given by Humphreys & Hirsch (1968) and Radi (1970) for a range of crystal structures. A comparison of measured and experimental values for Al, Cu, Au, Si, Ge, MgO and NaCl is given by Weickenmeier & Kohl (1991). A Fortran program for computing the phonon-scattering contribution to the absorption coefficients is also described by Bird & King (1990), together with tabulated values for Al, Cu, Ag, Au, C and Ga. Measurements for CaF_2 are given by Ichimiya & Lehmpfuhl (1988), based on an analysis of the spot splitting seen in wedge crystals. (These may be the most accurate experimental measurements available.)

The Fourier coefficients of the elastic portion of the optical potential for a centric crystal are (in V)

$$V_{\mathbf{g}} = (h^2/2\pi\gamma m_0 e\Omega) \sum_i f_i^B(\mathbf{g}) \exp(-2\pi i \mathbf{g} \cdot \mathbf{r}_i) \times \exp(-B_i \mathbf{g}^2/4).$$

An atomic absorptive form factor $f_i'(\mathbf{g})$ can be defined similarly by

$$V_{\mathbf{g}}' = (h^2/2\pi\gamma m_0 e\Omega) \sum_i f_i'(\mathbf{g}) \exp(-2\pi i \mathbf{g} \cdot \mathbf{r}_i) \times \exp(-B_i \mathbf{g}^2/4)$$

where $V_{\mathbf{g}}'$ is the imaginary part of the Fourier coefficient of the optical potential. The 'atomic' absorption coefficient $f_i'(\mathbf{g})$ is then given by (Hall &

Hirsch, 1965)

$$f'(\mathbf{g}) = K \int f^B(\mathbf{q}) f^B(\mathbf{q}-\mathbf{g})[\exp(-B\mathbf{g}^2/4) - \exp\{-B[\mathbf{q}^2 - (\mathbf{q}-\mathbf{g})^2]/4\}]\, d^2\mathbf{q}.$$

The integral may be evaluated on a grid of B and $\mathbf{g}$ values (Bird & King, 1990) or analytically either by expanding the atomic scattering factor as a sum of Gaussians (Weickenmeier & Kohl, 1991) or by taking the Rutherford form for the important high-angle part, thus obtaining a closed-form result (Ichimiya, 1985).

Absorption coefficients may be measured using the intensity distribution in the zero-order disc of a CBED pattern at the Bragg condition. The phases of the Fourier coefficients of the absorption potential may be measured by comparing the intensities of the $\mathbf{g}$ and $-\mathbf{g}$ reflections near the Bragg condition. Examples of these measurements are given in §§ 3.1 and 3.2.

3. Techniques

3.1. *Quantitative CBED*

Many researchers have described structure-factor refinements based on fitting (30) to the rocking curves recorded in experiment convergent-beam (CBED) patterns. Figs. 1(*a*) and (*b*) show the principle of the CBED method in one dimension. Each point P within the (incoherently filled) final illumination aperture acts as an independent point electron emitter, which defines the direction of a plane wave at the sample. For sub-nanometer probes, the illumination may take the form of a coherent aberrated spherical wave. However, for perfectly crystalline slabs, the variation of intensity in the CBED rocking curve is then the same as for the incoherent case provided the orders do not overlap (Spence & Carpenter, 1986). A source point such as P gives rise to a set of scattered waves which reach the detector at a family of points such as P'. A different source point Q similarly results in a different family of diffracted beams Q'. Thus, each point in the central CBED disc corresponds to a different incident-beam direction and defines a family of conjugate points differing by reciprocal-lattice vectors, one in each CBED disc. These directions can be related to the Ewald-sphere construction as shown in Fig. 1(*b*).

In practice, the intensities of several orders near the Bragg condition must be compared with calculations for a range of incident-beam directions (K_x, K_y). A subset of inner structure factors is adjusted until the dynamical rocking curve fits the experimental result. Outer structure factors are taken from calculations for free atoms. A separate matrix diagonalization is required for each incident-beam direction, which defines a point on the rocking curve. The specimen thickness, absorption coefficients and

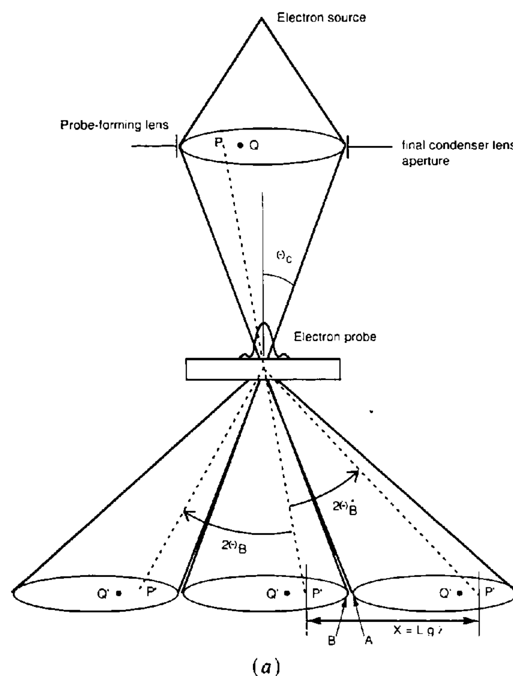

(*a*)

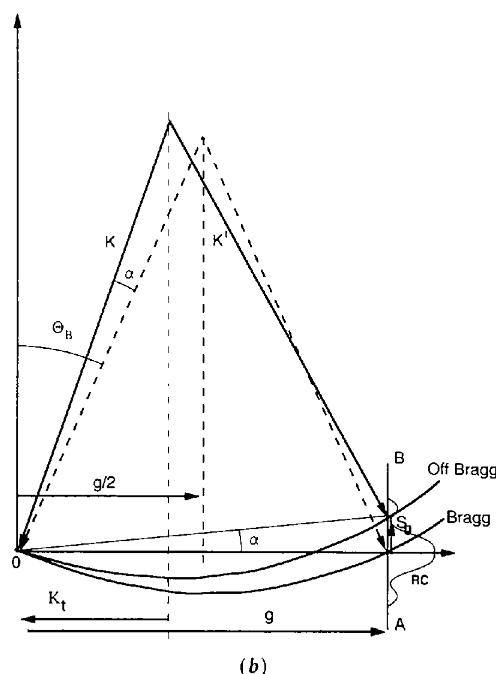

(*b*)

Fig. 1. (*a*) Simplified ray diagram for convergent-beam electron diffraction. If only elastic Bragg scattering is allowed, source point P gives rise to conjugate points P', one in each disc. Source point Q defines a different incident-beam direction and set of diffracted beams Q'. The camera length is L. (*b*) Two Ewald-sphere orientations differing by α, just off (continuous lines) and on (dashed lines) the Bragg condition. Note the direction of $\mathbf{K}_t$. The excitation error is S_g. In this simplified one-dimensional case, $S_g = 2\theta_B\alpha/\lambda = g\alpha$, where g is a reciprocal-lattice vector. Methods for calibration of the beam direction in two dimensions are given by Spence & Zuo (1992).

structure factors are all treated on an equal footing as adjustable parameters. Accelerating voltage is calibrated by comparing the pattern of HOLZ lines in the (000) CBED disc for silicon with dynamically corrected calculations for a sparse zone axis (Lin, Bird & Vincent, 1989; Zuo, 1992). For reviews of this work, see Cowley (1967) and Goodman (1978). Typical of this approach are the papers of Goodman & Lehmpfuhl (1967) and Avilov, Semiletov & Storozenko (1989) on MgO and Voss *et al.* (1980) on silicon. See also Høier, Zuo, Marthinsen & Spence (1988) for InP, Ishizuka & Taftø (1984) for ZnS, Kreutle & Meyer-Ehmson (1969) for Si, Marthinsen & Høier (1988), Shishido & Tanaka (1976) for Ge, Smart & Humphreys (1978) for Cu, Smith & Lehmpfuhl (1975), Steeds & Mansfield (1984), Terasaki, Watanabe & Gjønnes (1979) for Si and Gjønnes, Gjønnes, Zuo & Spence (1988) and Zuo, Spence & O'Keefe (1988) for GaAs.

The results of two- and three-beam theory can be used as a guide to find which regions of the pattern are most sensitive to changes in the structure factors. By differentiating the two-beam result with respect to each of the parameters t, U_g, λ and S_g it is found that the best sample thickness is the steepest part of the *Pendellösung* fringe (where intensity changes most rapidly with both thickness and structure factor), the best orientation for refinement of U_g is the Bragg condition for reflection **g**, while the three-beam degeneracy point gives greatest sensitivity for phase measurement (see § 3.2). For a given crystal, the adjustable parameters include t, U_g and choice of orientation. In the past, only the low-order structure factors of small-unit-cell crystals have been refined, for which the Debye–Waller factors and atomic coordinates were accurately known. It will be seen, however, that the automated refinement technique to be described can readily be generalized to refine other parameters, such as atomic coordinates, local strain and Debye–Waller factors.

First, consider the experimental conditions which provide the greatest sensitivity to changes in structure factors. The solutions to (26) and (30) if only two beams are admitted give the intensity I_g as a function of sample thickness t, structure factor U_g, accelerating voltage and excitation error S_g as

$$I_g = \frac{|U_g|^2 \sin^2 [(\pi t/K_n)(K^2S_g^2 + |U_g|^2)^{1/2}]}{K^2S_g^2 + |U_g|^2} \tag{31}$$

$$= |U_g|^2 \sin^2 (\pi t \Delta\gamma)/(K_n \Delta\gamma)^2 \tag{32}$$

with

$$I_0 = 1 - I_g.$$

Here $\Delta\gamma$ is the gap between the two-beam dispersion surfaces. The intensity minima occur at S_g values

$$S_g^2 = [n^2/t^2(K/K_n)^2] - |U_g|^2/K^2. \tag{33}$$

The thickness measured is the effective crystal thickness, $t^{\text{eff}} = t(K/K_n) = t/\cos\theta$, where θ is the angle between the beam direction and the surface normal. The intensity at the intensity maxima is given by

$$I_g = [\pi t |U_g|/K_n]^2/(1 + x^2), \tag{34}$$

where x is given by the solutions of $x = \tan x$. At the Bragg condition $s_g = 0$, the intensity becomes

$$I_g = \sin^2 (\pi t |U_g|/K_n). \tag{35}$$

The periodicity of the intensity with thickness when $S_g \neq 0$ is $L = \xi_g(1 + w^2)^{-1/2}$.

Fig. 2 shows the two-beam intensity function plotted as a function of both thickness and orientation. The dimensionless parameter $\omega = S_g\xi_g$ has been used, with $\xi_g = 1/(\lambda U_g)$. The position of minima in the rocking curve well away from the Bragg condition (S_g large) are more sensitive to changes in thickness than to changes in structure factor, due to the factor of n^2 in (33), and these minima are therefore used to determine sample thickness. Structure factors, however, are best determined from the ratios of the intensity maxima B/A shown in Fig. 2 at the Bragg condition for the reflection of interest and at one of the optimum thicknesses t_n. In practice, the value of t_n will be chosen to maximize the ratio of elastic to inelastic scattering. For $S_g = 0$, from (31), I_g is seen to be equally sensitive to t and U_g, so that the optimum thicknesses $t_n = \xi_g(n + 1/4) = (n + 1/4)K/U_g$ should be used where the slope of the thickness fringes is greatest. Thus, owing to the sine function in this equation, I_g can be very sensitive to changes in structure factor. For example, when $t|U_g|/K = 5/4$, a 1% change in u_g results in a 6% change in the B/A ratio. It is possible to obtain two Bragg conditions in a single systematics CBED recording, or more in two dimensions. For accurate

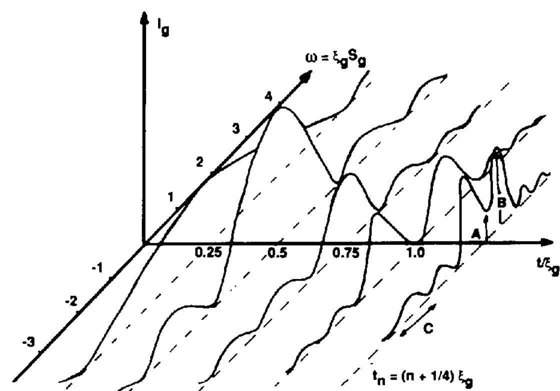

Fig. 2. The variation of the intensity of a diffracted beam with both thickness and incident-beam direction (represented by ω) in the two-beam approximation. Structure factors are best determined using the ratio of intensities A/B shown, at which thickness the sensitivity is greatest.

work, zero-loss energy-filtered data are required along the entire systematics line, in addition to photographic recordings for the determination of the approximate beam direction. This process must be repeated with each order to be refined successively set at the Bragg condition. Dynamical simulations of the HOLZ lines in the central disc (assuming reasonable values for the ionicities) will roughly calibrate the three-dimensional beam direction, however, this must also be refined for the most accurate work since changes in the low-order structure factors cause small shifts in the Bragg condition for HOLZ lines. [For an analysis of HOLZ-line displacements due to multiple scattering in the ZOLZ, see Bithell & Stobbs (1989), Lin, Bird & Vincent (1989) and Zuo (1992)]. Absorption parameters are most accurately refined using the variation of intensity within the central disc. Fig. 3 shows experimental data from MgO systematics reflections, recorded both on film and using a photomultiplier and serial energy-loss filter tuned to the elastic peak. Fig. 4 compares MgO results with dynamical calculations based on (30), after final refinement (Zuo & Spence, 1991).

We now consider the automation of the fitting process using a least-squares procedure. Since different parts of the rocking curve show different sensitivities to different parameters, the entire CBED refinement process is best handled by minimizing a weighted goodness-of-fit (GoF) index χ (Marthinsen, Høier & Bakken, 1990; Zuo & Spence, 1991), as in the Reitvedt method used in neutron diffraction. The refinement is thus accomplished by finding a minimum in χ^2 as a function of the adjustable parameters. We define

$$\chi^2 = \sum_i \frac{f_i(cI_i^{\text{theory}} - I_i^{\text{exp}})^2}{\sigma_i^2}. \tag{36}$$

The experimental CBED intensities are given by I_i^{exp} and the calculated points [from (30)] by I_i^{theory}. The f_i is a weight coefficient which can be adjusted to increase the importance of certain contributions to χ^2 which are sensitive to particular parameters. Here, σ_i^2 is the variance of the ith point, which can be measured from successive experiments or by using $\sigma_i^2 = I_i^{\text{exp}}$ if Poisson statistics are assumed. Further, c is a normalization coefficient, which can be found by either normalizing the theory and experiment at a particular point or by taking the first-order derivative of χ^2. This gives

$$c = \frac{\sum_i (f_i/\sigma_i^2) I_i^{\text{exp}} I_i^{\text{theory}}}{\sum_i (f_i/\sigma_i^2) I_i^{\text{theory}} I_i^{\text{theory}}}. \tag{37}$$

In a typical initial refinement for a centric crystal with, say, three CBED discs $(0, \mathbf{g}, \mathbf{h})$, one therefore performs a search in five-parameter space if absorption and thickness are included. (The zero-order absorption coefficient is not refined since it causes only a uniform exponential attenuation of all beams.) A separate diagonalization of the structure matrix is required for every data point, since each point in the rocking curve corresponds to a different incident-beam direction. This process must then be repeated for every set of parameters. The use of perturbation methods to increase computing speed is discussed below.

Since no optimization method can guarantee finding a global minimum in χ^2, it is necessary to

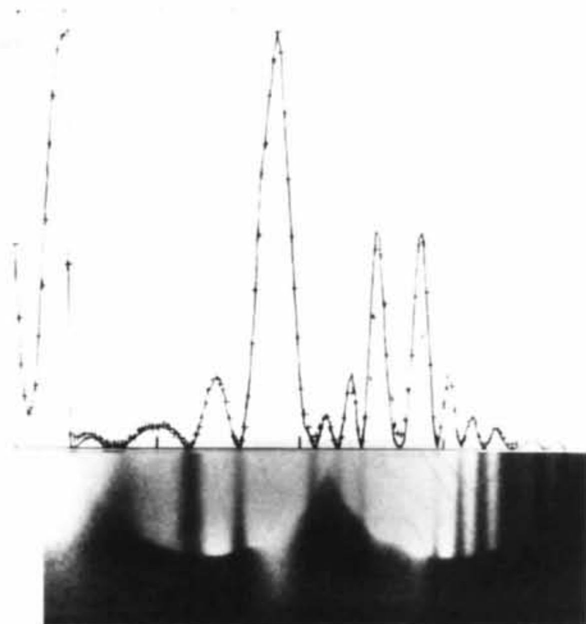

Fig. 3. A comparison of the [111] systematics at 120 kV for MgO recorded on film (below) with elastic energy filtering (crosses) and calculations refined for best fit (continuous line). A photomultiplier and serial energy-loss spectrometer were used.

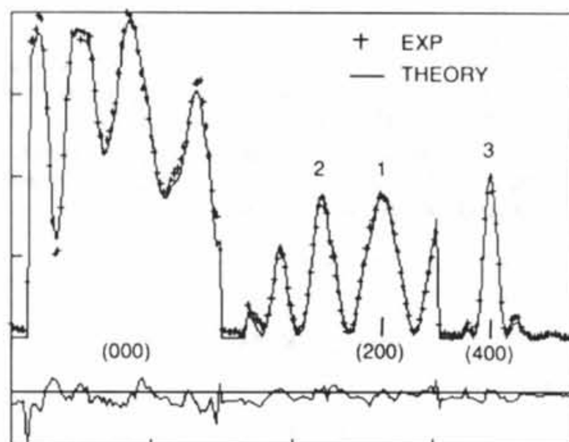

Fig. 4. Final refinement of MgO [h00] systematics at 120 kV. Dynamical calculations (continuous line), experimental data (crosses). Their difference is shown below. The Bragg conditions are indicated.

compare various optimization algorithms. A test of several algorithms suggests that the 'simplex' method is the most robust, if not the fastest, and has been consistently more successful in our work than other methods for finding global minima. A Fortran program (*REFINE/CB*) has been developed for this refinement and is available from the author or as part of the *XTAL* X-ray and neutron crystallography package (Hall, 1991). This is essentially a combination of the Bloch-wave program based on (30) with the *SIMPLEX* least-squares non-linear optimization program. The program is described by Zuo & Spence (1991). A flow chart is shown in Fig. 5. The optimization routine (subroutine *AMOEBA*) is discussed elsewhere (Press, Flannery, Teukolsky & Vetterling, 1986). The results for MgO shown in Fig. 4 were obtained using this program. The experimental conditions for this work were as follows: data were collected at 120 kV (nominal) from an MgO smoke crystal on a Phillips EM400 electron microscope using a 100nm probe and double-tilt stage to reduce contamination. The pattern was deflected under computer control over the entrance aperture of a Gatan model 607 serial energy-loss spectrometer (ELS). An energy window of 5 eV was used, centered on the elastic peak. The ELS entrance aperture size was 1 mm (giving an angular resolution of 0.15 mrad) and the camera length used was 6500 mm. The LaB_6 electron source used provided sufficient stability for the collection of 200 points, each with a dwell time of 100 ms. (Stability is checked by comparing counts at the same point before and after the scan.) The zero disc contained 68 points. The incident-beam direction was measured from Kikuchi-line features in the CBED pattern recorded on film, and later included in the refinement. The method used to define the scan coordinates is discussed in Zuo & Spence (1991). The initial thickness refinement was performed using nine systematic beams. Structure factors for neutral atoms were used, together with tabulated absorption coefficients (Bird & King, 1990). An initial structure-factor refinement was performed using nine systematic beams. Five parameters were adjusted – $U(200)$, $U'(200)$, $U(400)$, $U'(400)$ and thickness. 126 function

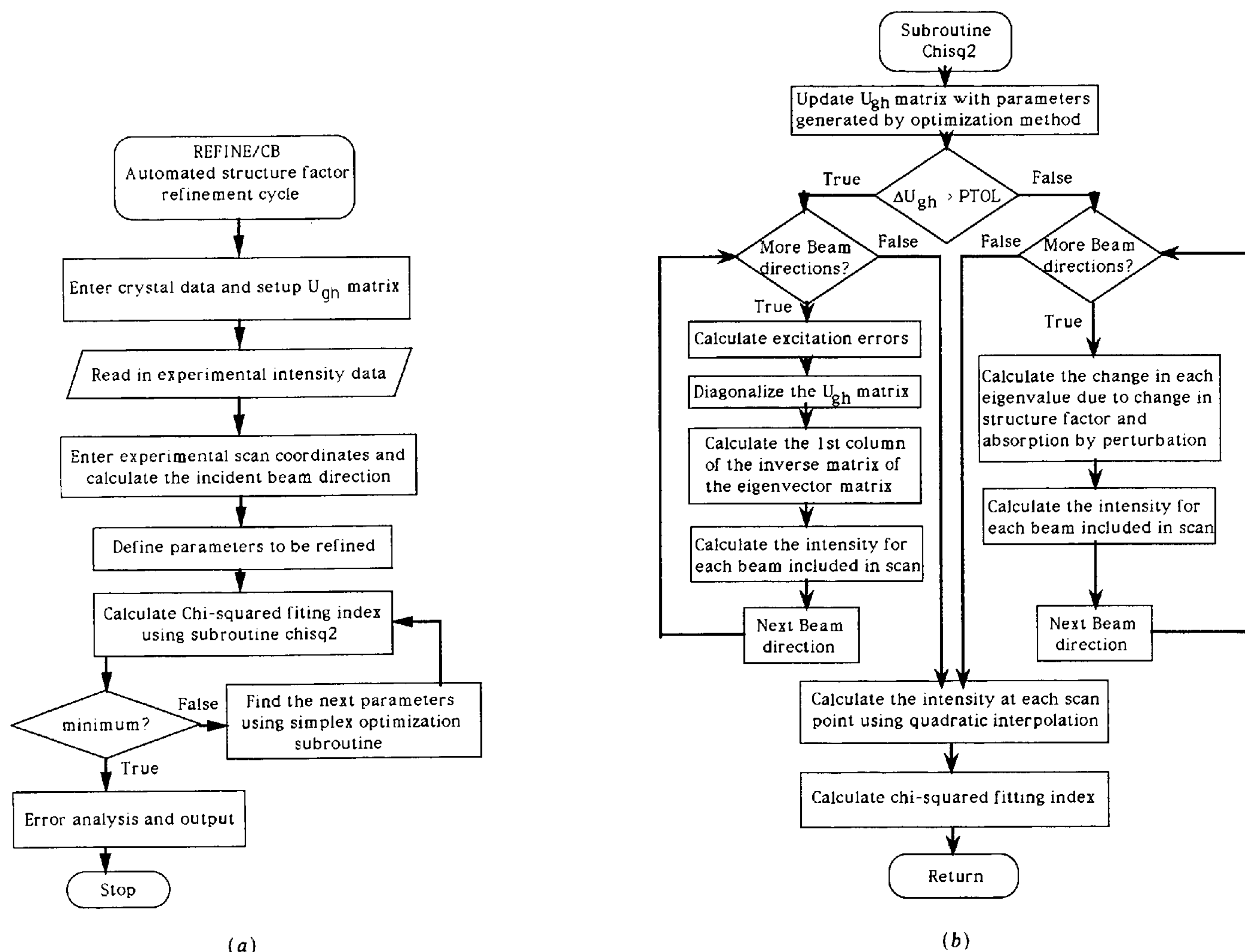

Fig. 5. (*a*), (*b*) Flow chart of the automated refinement program. (*a*) Main program. (*b*) Subroutine to evaluate χ^2.

evaluations were required for subroutine *AMOEBA* to reach the minimum, requiring 16 min 43 s processor time on a VAX station 3200 computer. The final refinement was performed using 33 beams, including HOLZ beams, and the same five parameters. A weight window was used with $f = 1.0$ for each point on the rocking curve except near the Bragg conditions of interest, where the refinement is most sensitive. Here $f = 20.0$. It took 84 function evaluations and a processor time of about 6 h to reach the minimum value of χ^2 on the VAX 3200 or about 1/4 of this time on the newer Silicon Graphics Indigo computer. The final results are given below with a discussion of the error analysis. Fig. 6 shows contours of equal χ^2 in the neighborhood of the minimum, plotted as a function of $U(200)$ and thickness for simplicity. The path chosen by the *SIMPLEX* algorithm is also shown for this simplified two-parameter refinement. It was found important to restart the *SIMPLEX* analysis from a different starting point in order to confirm that a global minimum had been found.

The procedure used for the subtraction of the background due to inelastic scattering is most important. This background consists of inelastic phonon scattering, plasmon scattering and losses due to electronic excitations. The use of an electron energy-loss spectrometer to collect only elastically scattered electrons (plus those which have excited phonons) considerably improves the accuracy of the refinement by eliminating the direct plasmon and single-electron excitation contribution. The removal of most of the Kikuchi pattern in two-dimensional elastically filtered CBED patterns, however, suggests that the dominant contribution to the background is the (large-angle) phonon scattering of (large-loss) plasmon-loss electrons. Thus, at the thicknesses which must be used for CBED work, multiple inelastic scattering is dominant. If filtering is not possible, densitometer scans taken just outside the CBED discs can also be used to estimate this phonon/plasmon diffuse scattering in the systematic case. This must be subtracted. Fig. 7(a) compares CBED patterns recorded with and without energy filtering on the new Zeiss EM912 Omega electron microscope (Mayer, Spence & Mobus, 1991), which incorporates an imaging energy-loss spectrometer into the electron–optical column. The elastically filtered pattern includes phonon-scattered electrons, but excludes those electrons which have excited plasmons, single-electron excitations and multiple combinations of these. The improved quality of the filtered data is clear from the densitometer traces shown in Fig. 7(c). (Even greater dynamic range is obtained using a filter and photomultiplier detector, as in Fig. 4.) Fig. 7(d) shows the remarkable amount of additional fine structure seen in wide-angle patterns, elastically filtered using the Omega filter.

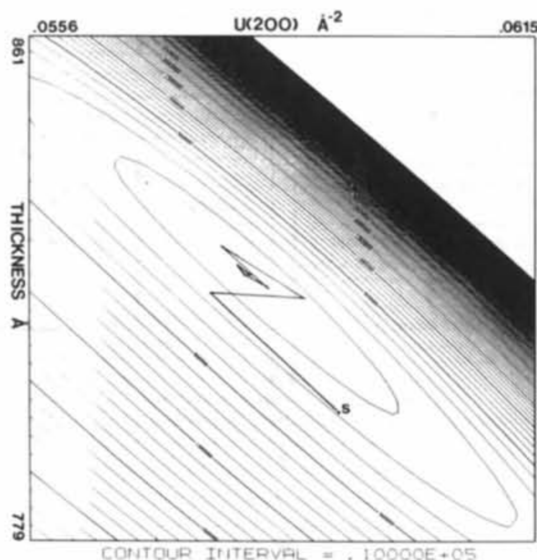

Fig. 6. Contours of constant χ^2 in two dimensions. For demonstration purposes, a refinement has been completed using only thickness and one structure factor as adjustable parameters. The path taken by the *SIMPLEX* algorithm to the minimum is shown by the continuous line from S. The contour increment is 10^4.

The use of perturbation methods in the *REFINE/CB* algorithm can reduce computing times dramatically. Most of the computing time (6 h on a VAX 3200) in the preceeding refinement was devoted to the final search, for which the diagonalization of a 33×33 complex matrix is required for each of the 68 data points, and this must be repeated for each of the four structure-factor parameters. For bonding and atomic-position-parameter studies, the structure matrix can be broken up into the sum of a zero-order matrix (including excitation errors) $\mathbf{A}_0$ and a smaller perturbation matrix $\mathbf{A}'$ containing the required changes in the structure factors due to bonding. The essential requirement for an absorption potential, however, complicates this somewhat since the matrix of eigenvectors is then not unitary. (For an acentric crystal with absorption it is neither symmetric nor Hermitian.) We assume that the eigenvectors are unchanged (Hirsch *et al.*, 1977). The changes in the eigenvalues due to a small change $\Delta U_{\mathbf{g}}$ in structure factors can then be obtained. If we retain only first-order terms, the change in the eigenvalues becomes

$$2K\Delta\gamma^i = \sum_{\mathbf{gh}} C^{-1}_{i\mathbf{g}} \Delta U_{\mathbf{gh}} C_{\mathbf{h}i}. \qquad (38)$$

$C_{\mathbf{h}i}$ is the eigenvector matrix of $\mathbf{A}_0$. $C^{-1}_{i\mathbf{g}}$ is the inverse matrix of the eigenvector matrix. If the percentage change in the structure factor ($|\Delta U_{\mathbf{gh}}|/|U_{\mathbf{gh}}|$) is smaller than a specified tolerance PTOL, then the perturbation method is used, otherwise the full diagonalization is used. The program updates the $\mathbf{A}_0$ matrix, its eigenvector matrix and the inverse of the eigenvector matrix if two successive cycles of the optimization routine

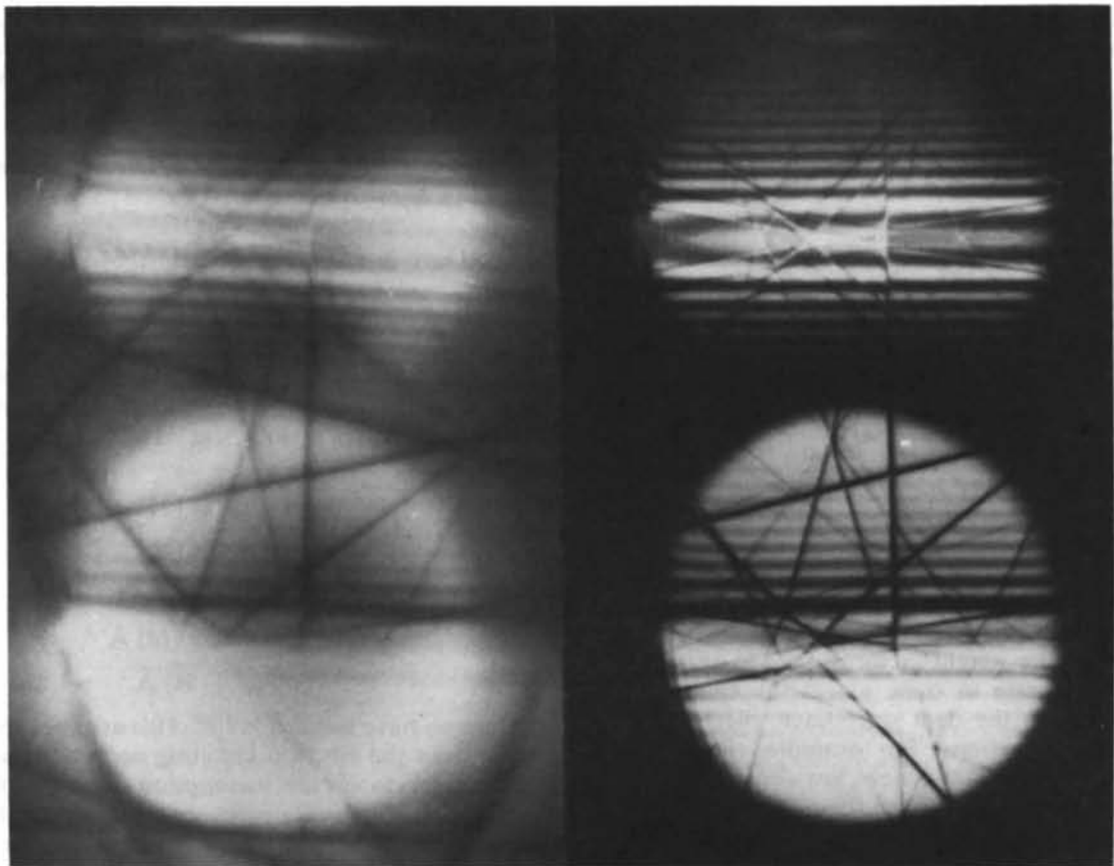

(a) (b)

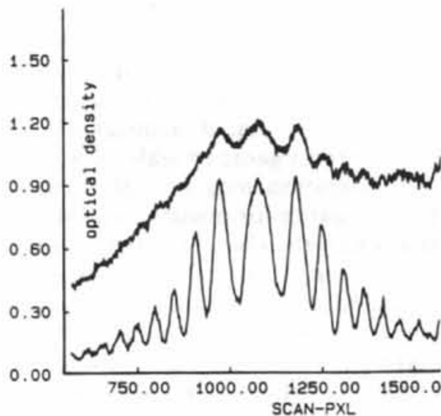

(c)

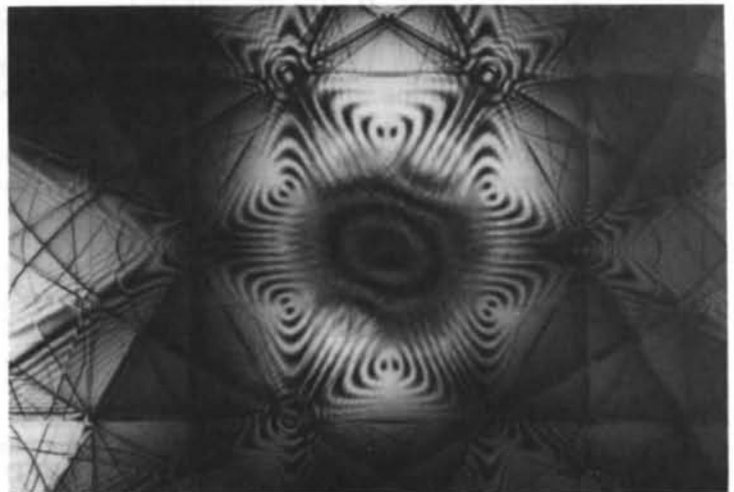

(d)

Fig. 7. (a), (b) Silicon (000) and (220) CBED discs recorded (a) without and (b) with the Zeiss Omega filter. The filter has been set to an 8 eV window around the elastic peak. Probe size 100 nm. Sample thickness about 270 nm. Apart from the introduction of the filter, no other changes were made to the experimental conditions (from Mayer, Spence & Mobus, 1991). (c) Densitometer traces taken from Figs. 6(a) and (b) showing the logarithm of the transmitted light intensity on the ordinate. Upper curve is without filter. Curve heights have been adjusted for approximately equal maximum optical density. (d) Large-angle CBED pattern (LACBED) recorded from the central disc of silicon in the (111) orientation using the Zeiss Omega filter at 100 kV. A very small selected-area aperture has also been used in a plane approximately conjugate to the source in order to minimize single inelastic phonon scattering, which is not otherwise removed by the filter. (Courtesy of J. Mayer, MPI, Stuttgart.)

result in a smaller χ^2 and the percentage change in the structure factor is larger than PTOL. Tests show that computing times are about equal for perturbation and diagonalization for a 9-beam refinement, however, the time for a 33-beam refinement with perturbation is 0.5 h rather than the 6 h required for diagonalization. For a noncentrosymmetric crystal, the neglect of changes in the eigenvectors may lead to significant error, as discussed in § 3.2. This procedure cannot therefore be used for the refinement of acentric crystals.

In summary, the automated refinement method makes it possible to refine many parameters, such as bonding reflections, positional parameters, temperature factors or lattice spacings for strain measurement from sub-micrometer regions using dynamical HOLZ line shifts (Zuo, 1992). However, the limitations of this technique have yet to be fully determined and difficulties will certainly be experienced with larger-unit-cell crystals unless wide-angle methods (Eades, 1984) can be used. This may entail some cost in probe size.

Through the weight factor, it should also be possible to separate to some extent the effects of the parameters on the data since each affects different groups of reflections. For example, the effects of bonding (which influence low-order reflections) might be disentangled from the position parameters, which, together with the Debye–Waller factors, affect mainly the high-order reflections.

Error analysis is all important in structure-factor refinement, since the effects sought are so small (Maslen, 1988). The accuracy of measurements made by the CBED method depends on the errors in all the parameters – thickness t, U_g (the assumed non-refined values), accelerating voltage E_0, electron counting noise, absorption coefficients U'_g and errors in the calibration of the incident-beam direction. In addition, it is essential to ensure that a sufficient number of beams have been included in the calculation, using convergence tests in which the number of beams is varied. We now investigate how errors in each of these parameters propagate through the dynamical scattering theory to affect the intensities. By differentiating the two-beam expression, we find that

$$(\Delta U_g/U_g)^2 = C_1(\Delta I_g/I_g)^2 + (\Delta t/t)^2 + 0.25(\Delta V/V)^2 + C_2(\Delta U'_g/U'_g)^2 \qquad (39)$$

where the values $C_1 \simeq 0.0$ and $C_2 = 0.01$ were obtained, for example, from computational trials for the 004 reflection in GaAs. Equation (39) is still useful if one or more parameters are found from other sources. For a least-squares fit with parameters a_k, we have (Bevington, 1969)

$$\sigma^2_{a_k} = \sum_{i=1}^{n} \sigma_i^2(\partial a_k/\partial I_i)^2. \qquad (40)$$

If a minimum in χ^2 is found and a parabolic expansion around the minimum can be made, the standard deviation is found to be (Wolberg, 1967)

$$\sigma^2_{a_k} \simeq [\chi^2/(n-p)]C^{-1}_{kk}. \qquad (41)$$

Here, C^{-1}_{kk} is the kth diagonal term of the inverse matrix of C which is defined by

$$C_{kl} = \sum_{i=1}^{n} (f_i/\sigma_i^2)(\partial I_i/\partial a_k)(\partial I_i/\partial a_l) = C_{lk}. \qquad (42)$$

These equations may be used to estimate the standard deviation in each parameter. The derivatives in (42) may be calculated by first-order perturbation theory. As an example, for the MgO refinement discussed above, we find, at 120 kV and room temperature,

$$U(200) = 0.05847\ (25),$$
$$U'(200) = 0.00158\ (4),$$
$$U(400) = 0.02484\ (48),$$
$$U'(400) = 0.00059\ (14)\ \text{Å}^{-2},$$
$$t = 808.0\ (54)\ \text{Å}.$$

Here we have used $\sigma_i^2 = I_i^{\exp}$. This assumes that the statistics of the electron counting noise are Poisson. Experiments to test this assumption suggest that deviations from Poisson statistics are encountered at large count rates when using a photomultiplier and scintillator.

3.2. *Solving structures*; *phase measurement*; *enantiomorphs*; *polarity*

Attempts to determine unknown crystal structures directly by electron diffraction have a long history. Early researchers, inspired by the success of the X-ray method, attempted to use kinematic scattering theory, especially in polycrystalline materials (Vainshtein, 1964), where it was hoped that dynamical effects would 'average out'. For inorganic crystals, considerable preliminary information may be collected in order to constrain the search for possible trial structures. CBED patterns may then be computed for each of these structures for comparison with experimental patterns. This preliminary information includes the crystal space group, the cell constants and angles and the number and type of atoms in the unit cell. Using CBED, point diffraction patterns and X-ray microanalysis, much of this information can be obtained, although with rather low accuracy. A serious problem arises with small crystals in the determination of the number of atoms in the cell, since there appears to be no way to determine the density of, say, a 10 nm crystalline precipitate. Other useful constraints are obtained from a table of interatomic bond lengths which occur commonly in nature and from atomic-resolution lattice images of the same structure.

The most comprehensive attack on the problem of structure determination by CBED is described by Vincent, Bird & Steeds (1984), who successfully determined the structure of AuGeAs precipitates at Au–Ge–In contacts on GaAs substrates. Their method was as follows. Isostructural crystals were grown and both these and the precipitates of interest were studied. The space group was determined from the symmetry of CBED patterns to be centrosymmetric, monoclinic, $C2/c$ (no. 15). Cell constants and angles were measured from spot patterns with an accuracy of about 0.5% and cell-constant ratios to higher accuracy (about 0.1%) using HOLZ lines. The NiP_2 structure, which has similar cell constants, angles and space group, was used as an early trial structure. From the space group, stoichiometry and likely tetrahedral coordination, it was concluded that either all atoms occupy separate fourfold sites or two species randomly occupy the $8(f)$ sites, with the third element on a fourfold site. The structure is then defined by the three positional parameters $\mathbf{r}=(x, y, z)$ defining the $8(f)$ site containing Ge and As atoms.

Many possible structures were then eliminated using bond-length arguments. Dispersion surfaces were then calculated for different values of $\mathbf{r}$, from which thickness-independent conclusions could be drawn about the width and visibility of HOLZ lines. The intensities of HOLZ reflections were then graded on a three-point scale and compared with calculations. (In thin crystals, because of their long extinction distances, the intensities of these reflections are relatively insensitive to thickness.) Reflections in widely differing projections were used, providing a severe three-dimensional test of the model. Voltage-dependent features were sought in the zone-axis orientation at which dispersion surfaces cross. The structure was finally confirmed to be isostructural with NiP_2 and PdP_2.

Approaches to generalizing the preceeding approach have also been discussed (Vincent, Bird & Steeds, 1984). Here, a conditional projected potential is introduced which involves a sum over Fourier coefficients in only one HOLZ layer. The transverse eigenstates can then be treated as atomic-like states, following the LCAO method of band theory (Buxton & Tremewan, 1980) and labeled accordingly as $1s$, $2p$ *etc.* according to symmetry. These states may be either bound or free, depending on how their transverse eigenenergy compares with the maximum in the interatomic potential. The aim of this work is to relate the intensities of HOLZ lines to modified structure factors, perturbed by the strong ZOLZ dynamical interactions. The choice of zone axes needed to distinguish trial structures with different numbers of free parameters is discussed in detail in Vincent *et al.* (1984) and Buxton & Tremewan (1980). The value of using HOLZ intensities for structure analysis emerges clearly from this work.

Recent work on structure analysis using the dynamical theory applied to point diffraction patterns can be found in Avilov *et al.* (1989), where crystals of LiF, PbSe, BiOCl, PbTe and Bi_2Se_3 are analyzed. A review of this work in English can be found in Cowley (1992).

In non-centrosymmetric (acentric) crystals, the determination of atomic coordinates requires a knowledge of the phases of structure factors. We therefore devote the remainder of this section to the methods which have been developed for measuring the phases of structure factors accurately by electron diffraction and to the closely related questions of enantiomorphs and polarity determination. For a review of corresponding work based on multiple-scattering effects in X-ray diffraction, see Chang (1987). [By comparison with X-ray work, electron diffraction has achieved much greater accuracy in structure-factor phase measurement but, unlike X-ray work, has until recently been restricted to small-unit-cell crystals, in order to avoid overlap of CBED orders. New techniques, such as low-angle convergent-beam electron diffraction (LACBED) and combination with lattice imaging may ease this restriction.]

For acentric crystals, we now let $U^c_{\mathbf{g}}$ be the complex electron structure factors (*i.e.* the Fourier coefficients) of the real part of the real-space optical potential and $U'_{\mathbf{g}}$ those of the imaginary part of the real-space optical potential. We note that, from (14), the phase of the electron structure factor $U^c_{\mathbf{g}}$ is not equal to that of the X-ray structure factor $F^x_{\mathbf{g}}$, but values of $F^x_{\mathbf{g}}$ can be determined from measurements of $U^c_{\mathbf{g}}$ and $U'_{\mathbf{g}}$. Since both are the complex Fourier coefficients of real real-space potentials, $U^c_{\mathbf{g}}=U^{c*}_{-\mathbf{g}}$ and $U'_{\mathbf{g}}=U'^{*}_{-\mathbf{g}}$. In general, it therefore becomes necessary to refine four numbers for each structure factor. In order to refine $U^c_{\mathbf{g}}$ and $U'_{\mathbf{g}}$, it will be found necessary in general to use rocking-curve data from both the $\mathbf{g}$ and $-\mathbf{g}$ reflections. Let $U^c_{\mathbf{g}}(\mathrm{Re})$ and $U^c_{\mathbf{g}}(\mathrm{Im})$ be the real and imaginary parts of the Fourier coefficients of the elastic real-space potential in an acentric crystal, with similar primed quantities for the absorption potential. Then the Fourier coefficients of the total complex optical potential obtained from a refinement program are

$$\begin{aligned} X(\mathbf{g}) &= U^c_{\mathbf{g}}(\mathrm{Re})+iU^c_{\mathbf{g}}(\mathrm{Im})+i\{U'_{\mathbf{g}}(\mathrm{Re})+iU'_{\mathbf{g}}(\mathrm{Im})\} \\ &= \{U^c_{\mathbf{g}}(\mathrm{Re})-U'_{\mathbf{g}}(\mathrm{Im})\}+i\{U^c_{\mathbf{g}}(\mathrm{Im})+U'_{\mathbf{g}}(\mathrm{Re})\}. \end{aligned}$$

If the complex value of $X(-\mathbf{g})$ can also be determined, it is possible by addition and subtraction to recover the required values of the complex $U^c_{\mathbf{g}}$ and $U'_{\mathbf{g}}$.

It is clear that the single-scattering or kinematic theory of diffraction does not allow phases to be measured nor, since (31) contains only $|U^c_{\mathbf{g}}|^2$, does the two-beam dynamical theory. The phase of $U^c_{\mathbf{g}}$

depends on the choice of origin in the crystal, but Kambe (1957) was able to show that the dynamical three-beam intensity depends only on a certain sum of the three relevant structure-factor phases, known as the three-phase structure invariant Ψ. Here

$$\Psi = \varphi_{\mathbf{h}} + \varphi_{-\mathbf{g}} + \varphi_{\mathbf{g}-\mathbf{h}}. \tag{43}$$

We note that the reciprocal-lattice vectors form a closed triangle and the quantity ψ is independent of the choice of origin in the crystal. Following Kambe's work, Gjønnes & Høier (1971) showed that, in the general non-systematics three-beam geometry for centric crystals, two special points exist on the hyperbolae defining the three-beam Bragg condition at which the intensity is zero due to a degeneracy in the eigenvalues. The position of zero intensity (or of a minimum in n-beam theory) indicates immediately whether the three-phase invariant is 0 or π for centric crystals. The position of this minimum depends also on accelerating voltage. Thus, for a centric crystal, it may be possible to determine whether the three-phase invariant is 0 or π by inspection of the position of the minimum in three-beam CBED patterns (Gjønnes & Høier, 1971; Hurley & Moodie, 1980).

For non-centrosymmetric crystals, experimental phase measurements have been reported by Bird, James & Preston (1987), Ichimiya & Uyeda (1977), Zuo, Spence, Downs & Mayer (1992), Zuo, Høier & Spence (1989), Zuo, Spence & Høier (1989) and others, whose work we now briefly discuss.

The first attempt to measure low-order structure-factor phases experimentally by dynamical electron diffraction appears to be that of Ichimiya & Uyeda (1977). Here (0002) thickness fringes from a 60° wedge in CdS were compared with calculations. As a result of the many-beam interactions, the intensity is sensitively dependent on structure-factor phase. The authors give an error of 0.04 for their measurement of $\tan\varphi$ (0002) = −0.54.

The three-beam non-systematic CBED method appears to be the most versatile and general method of phase determination, since it requires neither wedge-shaped samples nor continuously variable electron wavelength, as in critical-voltage methods. We assume that only beams **0**, **g** and **h** are excited. The method depends on an analysis of the intensity along the hyperbolic lines of maximum intensity in three-beam CBED patterns, such as those shown experimentally in Fig. 8. On these hyperbolae, the incident beam is constrained by the geometry of the (dynamical) Bragg condition to move such that

$$2KS_{\mathbf{g}} = |U_{\mathbf{g}-\mathbf{h}}|^2/2KS_{\mathbf{h}}. \tag{44a}$$

The experimental geometry and theory is given in detail in Zuo, Høier & Spence (1989). The hyperbolae are asymptotic to the Bragg lines $S_{\mathbf{g}}=0$ and $S_{\mathbf{h}}=0$. Along the lines of maximum intensity, Kambe's approximation may be used to give an expression for the intensity:

$$I_{\mathbf{h}}(S_{\mathbf{g}}) = \{(2KS_{\mathbf{g}})^2/[(2KS_{\mathbf{g}})^2 + |U_{\mathbf{h}-\mathbf{g}}|^2]\} \times \sin^2\{(\pi t/K)|U_{\mathbf{h}}^{\rm eff}|\}. \tag{44b}$$

Here,

$$|U_{\mathbf{h}}^{\rm eff}|^2 = |U_{\mathbf{h}}|^2 \frac{(2KS_{\mathbf{g}})^2}{|U_{\mathbf{h}-\mathbf{g}}|^2 + (2KS_{\mathbf{g}})^2} \times \left\{\left(1 - \frac{|U_{\mathbf{g}}||U_{\mathbf{h}-\mathbf{g}}|}{2KS_{\mathbf{g}}|U_{\mathbf{h}}|}\cos\Psi\right)^2 + \left(\frac{|U_{\mathbf{g}}||U_{\mathbf{h}-\mathbf{g}}|}{2KS_{\mathbf{g}}|U_{\mathbf{h}}|}\sin\Psi\right)^2\right\}. \tag{44c}$$

The expression for the intensity of reflection **g** is obtained by interchanging **g** and **h** in (44b) and (44c). The effective potential here is the same as the Bethe potential [(50)] if $2KS_{\mathbf{g}} \gg |U_{\mathbf{gh}}|$, which is the condition for the Bethe approximation. The change in excitation error measured along the line $S_{\mathbf{g}} = S_{\mathbf{h}}$ across the gap is found to be

$$\Delta S_{\mathbf{h}} = |U_{\mathbf{g}-\mathbf{h}}|/K. \tag{45}$$

This equation is the basis of the IKL (intersecting Kikuchi line) and IHL (intersecting HOLZ line) methods, since it offers a simple method of measuring $U_{\mathbf{g}-\mathbf{h}}$. This gap between the lines at the Bragg condition has been studied for many years since early work on Kikuchi-line patterns by Shinohara (1932). In X-ray diffraction it is known as the Renninger effect. It is this gap which is measured in the intersecting IKL and IHL methods described in § 3.4.

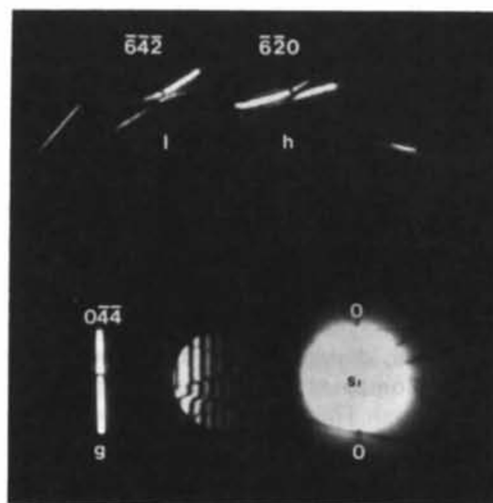

Fig. 8. Non-systematic three-beam CBED pattern from silicon recorded at 100 kV. The two beams at the Bragg condition **l** = $\bar{6}\bar{4}\bar{2}$ and **h** = $\bar{6}\bar{2}0$ differ by the $0\bar{2}\bar{2}$ reflection containing vertical bands. The gaps in the intensity along the Bragg hyperbolae in reflections **l** and **g** can be seen.

The position of the maxima and minima of intensity along the hyperbolae depend on Ψ and are given by (Zuo, Høier & Spence, 1989)

$$S_{\mathbf{h}} \simeq \frac{|U_{\mathbf{g-h}}|}{4K \cos \Psi} \left\{ \frac{|U_{\mathbf{h}}|}{|U_{\mathbf{g}}|} - \frac{|U_{\mathbf{g}}|}{|U_{\mathbf{h}}|} \pm \left[\left(\frac{|U_{\mathbf{h}}|}{|U_{\mathbf{g}}|} - \frac{|U_{\mathbf{g}}|}{|U_{\mathbf{h}}|} \right)^2 - 4 \cos^2 \Psi \right]^{1/2} \right\}. \quad (46)$$

Thus, the value of the three-phase sum can be determined from measurements of the position of the minimum. This minimum occurs on the lower hyperbola if cos Ψ is positive and on the upper branch if cos Ψ is negative. The distance between the maximum and the minimum intensities on the three-beam hyperbolae is

$$d = s_{\mathbf{h}}^{\max} - s_{\mathbf{h}}^{\min} = \frac{|U_{\mathbf{g-h}}|}{2\kappa \cos \Psi} \left[\left(\left| \frac{U_{\mathbf{g}}}{U_{\mathbf{h}}} \right| - \left| \frac{U_{\mathbf{h}}}{U_{\mathbf{g}}} \right| \right)^2 + 4 \cos^2 \Psi \right]^{1/2}. \quad (47)$$

The phase may then be found since

$$|\cos \Psi| = \left(\left| \frac{U_{\mathbf{g}}}{U_{\mathbf{h}}} \right| - \left| \frac{U_{\mathbf{h}}}{U_{\mathbf{g}}} \right| \right) \Big/ 2 \left(\frac{d^2 K^2}{|U_{\mathbf{gh}}|^2} - 1 \right)^{1/2}. \quad (48)$$

The sign of cos Ψ is indicated by the positions of the maxima and minima. Distances measured on film must first be converted to excitation errors. Using this method, Bird, James & Preston (1987) and Bird & James (1988) have measured the $\bar{3}7\bar{5}, \bar{1}7\bar{9}, \bar{2}04$ phase triplet in InP to an accuracy of ±15°.

A third paper (Zuo, Høier & Spence, 1989) also uses the non-systematic three-beam geometry. For CdS, these workers used many-beam calculations to match the intensity along lines across the $41\bar{4}$ hyperbolae. The $41\bar{2}$ reflection was also excited. The result of their analysis gives the sum of the phases of these electron structure factors, together with that of the $00\bar{2}$, to be 49.6 (5)°. Data were recorded on film and read into a computer for comparison with dynamical calculations. Allowance must be made for the logarithmic response of the film (Valentine, 1966). The background was accounted for by convoluting the computed intensity with a model distribution for inelastic scattering. If it were assumed that two of these phases were known exactly, the error in the remaining $00\bar{2}$ X-ray structure factor was found to be ±0.75°.

The fourth case concerns measurements made in the systematic orientation, based on a similar principle to that of the critical-voltage method, but extended to non-centrosymmetric crystals (Zuo, Spence & Høier, 1989). The principle of the method is as follows. As in the critical-voltage method, we consider a second-order reflection **g** at the Bragg angle in an acentric crystal. For a certain range of accelerating voltage, the perturbation to the rocking curve for the second-order reflection **g** due to the unavoidable weak excitation of the first-order reflection **h** is shown below to be very sensitive to the sum of the phases of the two relevant structure factors. (Excitation of the third-order beam is much weaker.) By comparison of the second-order beam's rocking curve with the results of many-beam calculations (including non-systematic interactions for increased accuracy), the phase sum may be found. Bethe's perturbation method may be used to analyze the method. With structure-factor phases $\varphi_{\mathbf{g}}$, the three-phase invariant for the $00h$ systematic in CdS becomes

$$\Psi = -\varphi_{\mathbf{g}} + \varphi_{\mathbf{h}} + \varphi_{\mathbf{g-h}} = -\varphi(00\bar{4}) + \varphi(00\bar{2}) + \varphi(00\bar{2}) = 2\varphi(00\bar{2}) - \varphi(00\bar{4}). \quad (49)$$

Unlike the non-systematics three-beam case, only two phases are now involved. The rocking-curve intensity observed in a CBED disc is given by (31) with $U_{\mathbf{g}}$ replaced by an effective structure factor

$$|U_{\mathbf{g}}^{\text{eff}}(B)|^2 = |U_{\mathbf{g}}|^2 \left\{ 1 - \frac{|U_{\mathbf{h}}||U_{\mathbf{g-h}}|}{\kappa S_{\mathbf{h}} |U_{\mathbf{g}}|} \cos \Psi + \left(\frac{|U_{\mathbf{h}}||U_{\mathbf{g-h}}|}{2\kappa S_{\mathbf{h}} |U_{\mathbf{g}}|} \right)^2 \right\} \quad (50)$$

to take account of the perturbation due to the third beam. The intensity now depends on Ψ. A plot of $|U_{\mathbf{g}}^{\text{eff}}/U_{\mathbf{g}}|$ for various values of the phase Ψ may be made. This shows that $|U_{\mathbf{g}}^{\text{eff}}|$ is most sensitive to changes in Ψ near its minimum

$$\left\{ \frac{|U_{\mathbf{g}}^{\text{eff}}(B)|}{|U_{\mathbf{g}}|} \right\}_{\min} = |\sin \Psi| \quad \text{for} \quad 2\kappa S_{\mathbf{h}} = \frac{|U_{\mathbf{h}}||U_{\mathbf{g-h}}|}{|U_{\mathbf{g}}| \cos \Psi}. \quad (51)$$

Thus, to obtain sensitivity to phase in disc **g** near $S_{\mathbf{g}} = 0$, we require $S_{\mathbf{h}}$ to satisfy the (material-dependent) constant of (51). We now use a similar argument to that used for the critical voltage. If $S_{\mathbf{g}} = 0$ then the Ewald-sphere geometry requires $2\kappa S_{\mathbf{h}} = \mathbf{h}^2$ in (51). Using the definition of $U_{\mathbf{g}}$ to solve for γ and the expression $E_0 = m_0 c^2 (\gamma - 1)/|e|$ for accelerating voltage, we find the accelerating voltage

$$E_A = \frac{m_0 c^2}{|e|} \left[\left(\frac{h^2 h_p^2 |V_g| \cos \Psi}{|V_h||V_{g-h}| 2 m_0 |e|} \right) - 1 \right] \quad (52)$$

where h_p is Planck's constant and **h** is a reciprocal-lattice vector. This equation reduces to an approximate form of the critical-voltage formula for $\Psi = 0$ or π (for centric crystals). The critical voltage corresponds to a choice of E_0 which makes $|U_{\mathbf{g}}^{\text{eff}}(B)| = 0$. Here we have extended the theory to acentric crystals and found the voltage E_0 at which, for a given phase, $U_{\mathbf{g}}^{\text{eff}}$ is a minimum near $S_{\mathbf{g}} = 0$, and therefore most sensitive to phase. Since, however, the excitation error $S_{\mathbf{h}}$ is used as a variable in CBED experiments, the choice of accelerating voltage is no longer critical. Unlike the critical-voltage method (which is restricted

to centric crystals), this method also allows independent refinement of several reflections, rather than giving a relationship between structure-factor amplitudes.

As an example, for CdS, with $\mathbf{g} = 00\bar{4}$ and $\mathbf{h} = 00\bar{2}$, $|U_\mathbf{h}| = 0.0577$, $|U_\mathbf{g}| = 0.0142$ and $\Psi = 55.332°$ for neutral atoms (room temperature, $E_0 = 120$ kV). Then, at $S_\mathbf{g} = 0$, a 1° change in Ψ leads to a 1% relative change in $U(00\bar{4})^{\mathrm{eff}}$. This produces a readily detectable change in $I_{\bar{\mathbf{g}}}$. Equation (51) also shows how insensitive the $00\bar{4}$ intensity is to $|U(00\bar{4})|$ and how sensitive it is to $|U(00\bar{2})|$. Thus (and in view of the relatively large size of $\mathbf{g}$), the use of scattering factors for neutral atoms (rather than ions) is a good approximation for $|U(00\bar{4})|$. Based on this approach, but using many-beam computations for greater accuracy, Zuo, Spence & Høier (1989) were able to refine Ψ for CdS from experimental CBED data, using the $00\bar{4}$ rocking curve. For the best fit it was found that

$$\Psi = 54.4\ (9)°.$$

The error is obtained from a quadrature sum of the phase changes due to errors in intensity measurement, the measured $|U_\mathbf{g}|$, absorption factors and thickness. If we assume $\varphi(00\bar{4}) = 2.94°$ (known), the corresponding error in the deduced X-ray structure-factor phase $\varphi^x(00\bar{2})$ is $\pm 0.069°$.

It is possible to convert these errors in the measurement of structure-factor phases to changes in atomic-position parameter if a degree of ionicity can be assumed. For CdS (a one-parameter structure), the preceding error makes it possible to determine the dimensionless atomic-position parameter to within about ± 0.0005. These ionicity and atomic-coordinate effects might be disentangled from a series of patterns emphasizing different orders. For example, we find that the 004 structure-factor phase is very sensitive to the position parameter u, whereas the phase of the 002 depends more strongly on bonding.

As a final example of structure-factor phase measurement, the 002 reflection in the noncentrosymmetric BeO crystal structure has been measured (Zuo, Spence, Downs & Mayer, 1993). BeO has the wurtzite structure, space group $P6_3mc$, with cell parameters $a = 2.6979$ (2) and $c = 4.3772$ (2) Å (Downs, Ross & Gibbs, 1985). The z parameter used was 0.3775. We choose an origin at the lighter Be atom. The polarity of the crystal was defined such that a vector drawn from Be to O is the positive [00.1] direction.

This example shows how the automated refinement techniques described in § 3.1 may be applied to acentric structures to determine individual phases (with respect to a specified origin) rather than phase sums. We will also see how the same values of the structure factors are obtained after analyzing crystals of different thicknesses. In this work, the origin was taken at the Be-atom site. Zero-loss filtered data were recorded at 80 kV using a serial ELS system fitted with a photomultiplier. Line scans were taken along the [00h] systematics near the [$\bar{1}$30] zone. As shown in Fig. 9(a), it was possible to obtain both the 002 and 004 Bragg conditions in the central disc, and this condition was used for refinement of the $U(200)$ amplitude $|U(200)|$, the $U(200)$ phase and the amplitude of the absorption coefficient $|U'(002)|$. Fig. 9(b) shows similar data taken from a different thickness of the same crystal. The refinement of the phase of $U'(200)$ was made using an axial orientation (not

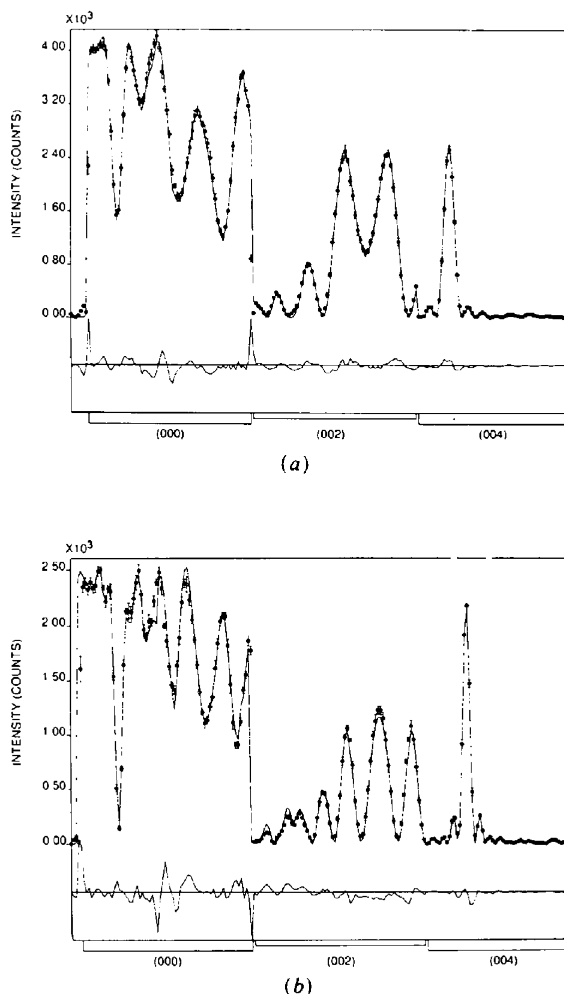

Fig. 9. BeO at two thicknesses. (a) Zero-loss experimental and computed CBED intensity along [002] in the central disc for BeO at 80 kV. The 002 and 004 Bragg conditions are indicated. The orientation is near the [130] zone axis. Refined sample thickness $t = 70.929$ nm. The plot below shows the difference between calculation and experiment. (b) Similar to Fig. 7(a) but recorded from a different thickness, found after refinement to be $t = 106.03$ nm. The close agreement between the structure factors retrieved from these two figures gives confidence in the method.

shown), in which both the 002 and 00$\bar{2}$ reflections were obtained at their Bragg conditions in a single CBED recording. Here, use is made of the fact that the difference in the intensity of the **g** and −**g** reflections in an acentric crystal is sensitive to the difference between the phases of the structure factors of the elastic and absorption potentials (Bird, James & King, 1989).

The data in Fig. 9 are shown compared with the results of many-beam Bloch-wave calculations. The calibration of the incident-beam coordinates and the determination of the center of the 000 disc are important in this work and these must be treated as refinement parameters in the *REFINE/CB* algorithm. Initial estimates were based on micrographs (two-dimensional data) taken with the scans, since these allow both components of the incident wave vector K_t in the ZOLZ to be determined. In particular, the x component of K_t, the center of the 000 disc and the thickness were refined together initially (refinement 1). About 20 search steps were needed to minimize χ^2. With these values, a further seven-beam refinement was made of thickness, $|U(002)|$, $\varphi(002)$, $|U'(002)|$ and $\varphi'(002)$ (refinement 2). These two refinements were then repeated until $\chi^2 = 5.04$. At this point, we have $t = 709.1$ Å, $|U(00.2)| = 0.039230$ Å^{-2}, $\varphi(00.2) = -0.89719$ rad, $|U'(002)| = 0.000755$ Å^{-2}, $\varphi'(002) = -0.62$ rad and $|U'(00.4)| = 0.000159$ Å^{-2}. A further reduction in χ^2 was then obtained by measuring the y component of K_t from micrographs, in order to include off-systematic reflections more accurately. The refinement was then continued (refinement 3) using 124-beam calculations (to include all reflections visible on the micrographs) and treating the complex $U(00.2)$, $U'(00.2)$, $|U'(004)|$ and t as adjustable parameters. Refinement 3 was then restarted, to confirm that a global minimum had been found. (This procedure is essential with the *SIMPLEX* algorithm.) This final refinement was done using 124 dynamically interacting beams, amongst which the 19 strong beams with small excitation errors were treated by exact matrix diagonalization, while the remainder of the weak beams were treated using the Bethe perturbation potential. The Debye–Waller factors used in this work were $B_{\text{Be}} = 0.355$ and $B_{\text{O}} = 0.28$.

For the measurement of the absorption phase $\varphi'(002)$, an axial 000 rocking curve was used. The acentric nature of the crystal was seen in the different heights of the 002 and 00$\bar{2}$ Bragg peaks obtained simultaneously in this pattern. Thus they are correctly normalized since they both occur within the 000 disc. A comparison with computations then allowed the polarity of the crystal and the absolute indexing of the pattern to be determined. The refinement of this pattern followed, using now $\varphi'(002)$ and thickness as refinement parameters, together with the values of $U(002)$ and $|U'(002)|$ obtained previously. The final values obtained at 80 kV, with $\chi^2 = 5.04$, were

$$|U(002)| = 0.039592\,(14)\ \text{Å}^{-2},$$
$$\varphi(002) = -0.8847\,(170)\ \text{rad},$$
$$|U'(002)| = 0.00073\,(6)\ \text{Å}^{-2},$$
$$\varphi'(002) = -1.1\,(5)\ \text{rad},$$
$$|U'(004)| = 0.0002\,(1)\ \text{Å}^{-2},$$
$$t = 711.6\,(16)\ \text{Å}.$$

Finally, the last refinement was repeated with a slightly different starting point, and the minimum thus confirmed to be unique. The polarity of the crystal was confirmed by repeating the analysis with every **g** replaced by −**g** in the computations. It should be noted that this reversal of polarity was found to increase χ^2 to about 20.

Considerable confidence in the method is given by comparing these values with those refined from Fig. 9(*b*), which shows data from the same crystal at a different thickness. The refinements from this figure give

$$|U(002)| = 0.03982\,(13)\ \text{Å}^{-2},$$
$$\varphi(002) = -0.8786\,(170)\ \text{rad},$$
$$|U'(002)| = 0.00090\,(7)\ \text{Å}^{-2},$$
$$\varphi'(002) = -0.4\,(5)\ \text{rad},$$
$$|U'(004)| = 0.00004\,(10)\ \text{Å}^{-2},$$
$$t = 1059.7\,(20)\ \text{Å}.$$

These fall within the errors of the previous analysis. The corresponding value of the X-ray structure-factor phase is obtained from (22) as $\varphi^x(00.2) = -1.1900\,(9)$ rad, corresponding to an accuracy of better than 0.1%. This may be the most accurate phase measurement yet reported by any method.

Reversing the sign of the phase of the plane wave representing the incident electron beam would reverse the sign of $\varphi(002)$, and this must be considered (together with the choice of origin) when comparing this work with results from other researchers.

A different group of techniques has been developed based on the straightforward measurement of the intensity of many high-order reflections, both in the ZOLZ and the HOLZ (Kolby & Taftø, 1991; Ma, Gjønnes & Taftø, 1991; Tomokiyo & Kuroiwa, 1990). In particular, the slight rotation of the oxygen octahedra which occurs during the phase transition in $SrTiO_3$ has been studied by Tanaka & Tsuda (1990), who use direct measurement of HOLZ reflections and comparisons with dynamical computations. Using a similar refinement technique, they were able to determine this rotation to within an accuracy of about 0.2°.

The 'handedness' or chirality of a crystal can be determined by analysis of CBED intensities. Space

groups differing in this way are known as enantiomorphs and are mirror images of one another. Note that two enantiomorphs may have either the same (*e.g.* point group 1) or different symmetry (as in the case of quartz). Applications of CBED for this purpose are described by Goodman & Johnson (1977) (for quartz) and for MnSi by Tanaka & Terauchi (1985). In both cases, the absolute orientation can be determined. The topic is also discussed by Vincent, Krause & Steeds (1986).

The effect of enantiomorphism on dynamical intensities has been analyzed by Marthinsen & Høier (1989). It can be understood by noting that any odd number of mirror operations reverses handedness and that three mirrors are equivalent to a center of inversion. The effect of replacing **r** by −**r** in the general expression for dynamical intensity may be understood by writing (30) as

$$I_{\mathbf{h}}(t)=\sum_i |C_0^{i*}C_{\mathbf{h}}^i|+2\sum_{i>j}|C_0^{i*}C_{\mathbf{h}}^iC_0^jC_{\mathbf{h}}^{j*}| \times\cos[+2\pi(\gamma_i-\gamma_j)^t+\alpha_{ij}], \qquad (53)$$

where α_{ij} is the phase of $C_0^{i*}C_{\mathbf{h}}^iC_0^jC_{\mathbf{h}}^{j*}$. The replacement of **r** by −**r** leaves the eigenvalues unaffected but conjugates all the eigenvectors. This reverses the sign of α_{ij}, which can lead to large intensity differences between the two crystals in CBED patterns along Bragg lines.

In three-beam theory, the effect of enantiomorphism is to reverse the phase of the three-phase invariant. From the three-beam expression (44*c*), we see that this does not lead to an observable effect within either the Bethe or Kambe approximations, unlike the exact three-beam solution (Marthinsen & Høier, 1989). In the wurtzite structure, the application of a mirror operation (or a twofold axis) reverses the polarity of the structure and we have seen above with BeO that the use of the incorrect polarity gave a much poorer refinement.

The effect of reversing the phase of the incident plane wave is to reverse both the sign of α_{ij} and the plus sign before the term $2\pi(\gamma_i-\gamma_j)$ in (53), so that the same intensity distribution is predicted from the same crystal, regardless of the plane-wave sign convention.

A simple CBED method, based on few-beam interactions, for determining the polarity of crystals with the sphalerite structure has been described by Taftø & Spence (1982). A second class of methods for determining polarity depends on asymmetries introduced into two-beam theory by absorption. If absorption is included exactly (not using perturbation theory), then small differences appear between the **g** and −**g** rocking curves in two-beam theory. These are responsible for asymmetries in Kikuchi lines (Allen & Rossouw, 1989; Bird, 1990; Bird & Wright, 1989) and on inner-shell energy-loss spectra (Taftø, 1987), both of which may also be used to determine the polarity of acentric crystals. (Energy 'absorbed' by inelastic processes from the elastic 'channel' makes a positive contribution to peaks in the energy-loss spectrum.)

3.3. *Critical voltages*

In its simplest form, the critical-voltage effect consists in the observation of a minimum of intensity in a second-order reflection at the Bragg condition for a particular accelerating voltage. This voltage depends sensitively on the ratio of the first- to second-order structure factors, and so may be used to measure this ratio with high precision from measurements of the critical accelerating voltage. If the second-order reflection is assumed to depend mainly on the known atomic coordinates, the first-order reflection, which is more sensitive to bonding effects, may be found with high precision. Accuracy is often ultimately limited by knowledge of the Debye–Waller factor for the high-order reflections and the contrast of the intensity minimum. Introductory reviews of the theory may be found in Cowley (1981), Humphreys (1979) and Reimer (1984). The first observations of the critical-voltage effect were made by Nagata & Fukuhara (1967), Uyeda (1968) and Watenabe, Uyeda & Kogiso (1968). The critical-voltage (CV) method is generally regarded as the most accurate method of structure-factor measurement by electron diffraction. What is usually measured is the ratio of the magnitude of the first-order structure factor $U_{\mathbf{h}}$ to that of the second-order reflection $U_{2\mathbf{h}}$ and the method requires an electron microscope whose accelerating voltage may be continuously varied over a large range, typically from 100 kV to 1 MeV. The field has recently been reviewed by Fox & Fisher (1988*b*).

The effect may be understood using either three-beam theory, based on the Bethe potentials (Uyeda, 1968), or from a (related) two-Bloch-wave picture (Lally, Humphreys, Metherell & Fisher, 1972). For example, the effective potential of (50) may be used in the two-beam expression (31) and the value of $\gamma=[1-(v/c)^2]^{-1/2}$ (and hence the accelerating voltage) found for which the effective potential is zero. For the centric crystals usually studied, $\Psi=0$ or π. The three-beam diffracted intensity is then zero for all specimen thicknesses. Alternatively, the exact solution of the symmetric three-beam case may be used. The critical-voltage effect then occurs at the eigenvalue degeneracy $\gamma^1=\gamma^3$. This condition is satisfied at the three-beam critical voltage

$$E_c=\frac{m_0c^2}{|e|}\left[\frac{h^2g^2|e|V_{2h}}{2m_0|e|^2(V_{\mathbf{h}}^2-V_{2\mathbf{h}}^2)}-1\right]. \qquad (54)$$

A critical voltage does not occur if $V_{\mathbf{h}}^2<V_{2\mathbf{h}}^2$. In the general many-beam case, this destructive interference between two Bloch waves for one particular beam

occurs when any two eigenvalues γ^j of the structure matrix **A** become degenerate for a particular voltage E_0. The symmetries of the two Bloch waves also interchange as E_0 passes through E_c. The problem has been analyzed in detail in the three-beam approximation for acentric crystals (Marthinsen, Matsuhata, Høier & Gjønnes, 1988).

The effects of accidental degeneracies in the eigenvalues has also been observed in the axial orientation by Matsuhata & Steeds (1987) at more conveniently lower voltages (see also Buxton & Loveluck, 1977). The effect may consist of a bright spot in the central disc of a zone-axis CBED pattern, or of a reversal of symmetry in the other orders. Five- and seven-beam closed-form solutions (reducible by symmetry) are used to analyze these results, together with many-beam calculations. Corresponding effects are found in the HOLZ reflections.

It was realized at an early stage that, since (50) contains the product $|\mathbf{K}|S_\mathbf{g}$, minima can be expected in CBED patterns for particular excitation errors at voltages other than E_c (which determines the wave vector $|\mathbf{K}|$). An error in choosing E_c may be compensated for by changing $S_\mathbf{g}$, *i.e.* by looking at a different point in the CBED pattern. This is the basis of the intersecting Kikuchi-line (IKL) method described in § 3.4, which might therefore be said to provide 'critical voltage at any voltage' (Taftø & Gjønnes, 1985). It is also the basis of the 'CBED critical voltage' method of Sellar *et al.* (1980). In this work, the temperature of the sample (and hence the Debye–Waller factor) was used for fine-tuning the critical-voltage condition. In general, degeneracies may be identified for certain combinations of excitation error and accelerating voltage by solving, in closed form, the few-beam dispersion equations. These solutions have now been given for many orientations of high symmetry (Fukahara, 1966). Intensity minima can therefore be found in many orientations of high symmetry, as analyzed in detail by Buxton & Loveluck (1977). The near extinction of a third-order systematic reflection is discussed by Hewat & Humphreys (1974).

In practice, by varying E_0, the experimentalist seeks the disappearance of the Kikuchi line associated with the satisfied Bragg beam (Thomas, Shirley, Lally & Fisher, 1974) or the central maximum of a dark-field bend contour (Lally *et al.*, 1972) or that of the central maximum of the rocking curve displayed in a CBED disc in the CBEDCV method (Sellar *et al.*, 1980). Many-beam dynamical calculations are then performed, in which the two lowest-order structure factors are adjusted to give a minimum of intensity in the second-order (satisfied) reflection for the observed value of E_c. Absorption coefficients must be known.

Table 2 contains a summary of measurements of structure factors made by the critical-voltage (and other) methods. Readers must be cautioned against comparing values recorded at different temperatures. Errors may be as small as 0.4% in the measured f_j values for Si(111) (Hewat & Humphreys, 1974), corresponding to an error of 0.11% in the corresponding X-ray scattering factor.

3.4. *The intersecting Kikuchi-line and HOLZ-line methods*

The critical-voltage method has the important advantage of being a 'null' method, in which a minimum of intensity is sought. Most electron diffraction methods depend on the direct measurement of electron intensities and their comparison with calculations. The intersecting Kikuchi-line (IKL) method is unusual in that it allows structure factors to be determined simply from the distance between features measured on a photographic plate. This distance is the width of the gap which appears when Kikuchi lines (or HOLZ lines) cross. We shall therefore also refer to the intersecting HOLZ-line (IHL) method.

Instead of following the geometric locus defined by the kinematic Bragg condition ($S_\mathbf{g}=0$), HOLZ lines separate where they cross. The resulting gap between the lines at the three-beam Bragg condition has been studied for many years since the first work of Shinohara (1932) on Kikuchi-line patterns. In X-ray diffraction, it is known as the Renninger effect. It is this gap which is measured in the IKL and related methods.

The situation can be analyzed with the aid of the three-beam dynamical theory for acentric crystals (Spence & Zuo, 1992). The gap (measured along the line $S_\mathbf{g}=S_\mathbf{h}$) between the hyperbolae defined by (44) is given by (45), and hence the structure factor $U_{\mathbf{g}-\mathbf{h}}$ can be obtained from a measurement of the gap.

The preceding results apply to elastic Bragg scattering. Similar gaps are seen in Kikuchi-line patterns. The assumption is made that the inelastic scattering responsible for Kikuchi lines is generated continuously throughout the crystal, and so can be described by an integration over thickness. This does not alter the expression for the gap.

A deeper understanding of both the critical-voltage and the closely related IKL methods can be obtained by plotting out the relevant many-beam dispersion surfaces for a range of incident-beam directions and accelerating voltages. The eigenvalues γ^i then describe the deviation of these surfaces from asymptotic spheres of radius $|\mathbf{K}|$ erected about each reciprocal-lattice point. This deviation is greatest near Bragg conditions. The surfaces may touch at certain accelerating voltages and orientations, giving rise to the CV and IKL effects. In three dimensions, the form of these surfaces can be very complicated.

The IKL and IHL techniques are simple to apply. However, the finding of suitable cases showing a clear

splitting unperturbed by other interactions at a convenient accelerating voltage is somewhat fortuitous, since a search through all possible diffraction conditions is rarely practical. The method is thus simpler and more flexible (if applicable) but less accurate than the critical-voltage method. An instructive case of high symmetry in which only one excitation error is varied is given by Taftø & Gjønnes (1985), applied to SiC. Other applications of the method can be found as follows: the concentration of V atoms at interstitial tetrahedral sites in vanadium oxide above the ordering temperature has been determined using structure-factor measurements based on the IKL technique by Høier & Andersson (1974). Structure factors for Cu and Cu_3Au have been measured using this method by Matsuhata, Tomokiyo, Watanabe & Eguchi (1984). Structure factors in silicon have also been measured by the IKL technique by Terasaki *et al.* (1979). The displacement of Kikuchi lines near intersections can also be understood using this approach (Høier, 1972).

3.5. *Weak high-order reflections*

Wide-angle methods which allow either kinematic or two-beam analysis of weak high-order reflections have been developed by Vincent & Bird (1986) and Taftø & Metzger (1985). We consider first the method of Taftø & Metzger. Consider a systematic row of reflections. The method depends on the fact that, because the extinction distances are large for high-order reflections, these reflections have very narrow rocking curves and, if the specimen thickness is much less than the extinction distance, may be described to a good approximation by two-beam or kinematic theory. The use of a systematic row also minimizes off-row dynamical interactions. In their study of a static displacement modulation in V_2D, Taftø & Metzger used a beam divergence many times greater than the first-order Bragg angle. Thus, many beams are simultaneously observed at the Bragg condition. But the beam divergence used is less than the Bragg angle for the high-order beams (*e.g.* 11,0,0) of interest. Thus, while the direct beam does not overlap with these beams, they do overlap amongst themselves. However, the contribution of an adjacent beam to one at the Bragg condition is small, since its excitation error is large. By comparing these sharp high-order systematic reflection intensities with kinematic calculations, Taftø & Metzger were able to measure the static modulation of the lattice as 0.0070 (5) nm. In a second application of the same method, Kolby & Taftø (1991) used high-order $00l$ reflections ($l = 8$ to 70) in intermetallic $Al_{11}Ti_4Zn$ to refine the atomic displacements of the Al and Ti atoms. An accuracy in the fractional coordinate of 0.006 (2) was achieved. The method has also been applied to the refinement of atom positions in Al_3Zr (Ma *et al.*, 1991). A third example of this approach is provided by the work of Boe & Gjønnes (1991), who compared the high-order $00l$ systematics in $YBa_2Cu_3O_{7-x}$ with calculations for three different models of oxygen ordering.

If the incident-beam direction is scanned electronically, it is possible to obtain an expanded angular view of the outer HOLZ lines (Kondo, Ito & Harada, 1984). It is also possible to obtain similar information without scanning from zone-axis patterns formed using an illumination semiangle equal to the angular radius α_1 of the first-order Laue zone (Vincent & Bird, 1986). Consider the effect of increasing the illumination semiangle θ_c on the ZOLZ and FOLZ reflections. The effect is to open up an annular band of FOLZ lines, centered around those which appear at the zone axis. At the same time, the ZOLZ becomes filled with a continuous distribution of bright overlapping orders. The use of $\theta_c = \alpha_1$ is shown to be an optimum condition, which prevents the zero-layer reflections from overlapping with the HOLZ, while also preventing overlap between reflections in different HOLZ. All electrons diffracted by planes in layer n of the reciprocal lattice are confined to an annulus whose inner and outer radii are α_n and α_{n+1}. Again, advantage is taken of the fact that the rocking curve for HOLZ reflections is very narrow owing to the steep inclination of the Ewald sphere as it crosses HOLZ lattice points. Thus, although different reflections in the same HOLZ overlap geometrically, the intensity contribution from neighboring reflections is negligible. (If orders overlap there is an intensity contribution to one point in the diffraction pattern from two different points within the illumination aperture, *via* different Bragg scattering paths.) In this case, one of the Bragg paths into the HOLZ from the source makes a negligible contribution because its excitation error is large and the lines are narrow due to the curvature of the Ewald sphere. Independently of this overlap effect, dynamical scattering between all the reflections normally occurs. The intensities of these lines, however, in the case of the silicon [114] pattern at 300 kV, are found to agree closely with electron structure factors, suggesting that a kinematic analysis of these intensities may be possible at some point along their length. The good fit may also be related to the use of a sparse (low-symmetry) zone, in which dynamical interactions are minimized.

4. The inversion problem

The inversion problem refers to the problem of finding values of U_g directly from measurements of the dynamical beam intensities, rather than by refinement based on forward computations. Two approaches have been made to this generally unsolved problem – firstly, based on closed-form inversion of few-beam solutions and, secondly, computational strategies in which algorithms are devised which might be shown to converge uniquely.

An analytical approach is given by Moodie (1979) for the three-beam case. Here, closed-form expressions are given for the retrieval of the three structure-factor amplitudes and the three-phase invariant from the positions of certain lines in a three-beam CBED pattern along which the intensity has two-beam form.

Several computational schemes have been tested in unpublished work by Spence & Katz (1979) (see also Speer, Spence & Ihrig, 1990). We write the scattering matrix defined following (29) in the form $\mathbf{S}=\exp(2\pi i\mathbf{A}t)$ for a centrosymmetric crystal without absorption. The problem then reduces to that of finding the entries $U_{\mathbf{g}-\mathbf{h}}$ of the structure matrix $\mathbf{A}$ from a knowledge of the moduli of the entries in one column of $\mathbf{S}$. We assume that the diagonal of $\mathbf{A}$ (the excitation errors), accelerating voltage and thickness only are known. Two cases might be considered: one in which the complex entries of one column of $\mathbf{S}$ have been determined [by interferometric methods, for example using a biprism in STEM (Cowley, 1991) or using coherent overlapping CBED orders (Spence, 1978)]; and one in which only the moduli of the elements are known. These data may be recorded as a function of thickness, orientation and accelerating voltage. The following general comments may be made for centric crystals without absorption:

1. The question of uniqueness arises. Let $\mathbf{S}=\exp(2\pi i\mathbf{A}t)=\exp(2\pi i\mathbf{B}t)$. Then uniqueness is established by showing that $\mathbf{A}-\mathbf{B}=0$. Since $\mathbf{A}$ and $\mathbf{B}$ are self-adjoint and diagonalized by the same eigenvectors, they commute and hence $\exp[2\pi i(\mathbf{A}-\mathbf{B})t]=\mathbf{S}\mathbf{S}^{-1}=\mathbf{I}$ for all t. This is only possible if $\mathbf{A}=\mathbf{B}$ and the inversion is thus unique if data are used for a range of thickness. (If it were not, in principle, two different structures could give rise to the same diffraction pattern. Then the inversion problem is not well posed.)

2. The eigenvalues of $\mathbf{S}$ are $\lambda_i=\exp(2\pi i\gamma_i t)=r\exp(i\theta_i)$. Hence,

$$2\pi i\gamma_i t=\ln\lambda_i=\ln r+i(\theta_i+2n_i\pi)$$

gives γ in terms of λ if the n_i are known, otherwise the inversion is not unique. If complex $\mathbf{S}$ can be found at several thicknesses (or non-relativistic wavelengths), the eigenvalues of $\mathbf{A}$ can then be found from the period in thickness $1/\gamma_i$ of the real part of λ_i. The eigenvectors of $\mathbf{S}$ are those of $\mathbf{A}$. Hence $\mathbf{A}$ can be found from $\mathbf{S}(t)$.

3. Many other physical constraints may be placed on the retrieval process and use can be made of other properties of the matrices (*e.g.* the trace of $\mathbf{A}$, related to the determinant of $\mathbf{S}$, is known *etc.*). So far, however, all these computational approaches to the inversion problem have foundered on the difficulty of reconstructing all of $\mathbf{S}$ from a knowledge of some of its entries.

The use of the difference between data recorded at two slightly different accelerating voltages has also been considered (Spence & Katz, 1979). In the non-relativistic regime in zone-axis orientations, the dynamical theory contains only the product λt, so that a small change in thickness t is equivalent to a small change in wavelength. A kinematic analysis might then be used if the data consisted of complex amplitudes.

5. The mean inner potential

A simple relationship has been shown to exist between the mean inner potential V_0 and the diamagnetic susceptibility (Miyake, 1940). For a monoatomic crystal consisting of atoms on lattice sites i with unit-cell volume Ω, the Fourier coefficients $V_{\mathbf{g}}$ of potential in SI units are

$$V_{\mathbf{g}}=\Omega^{-1}\sum_i f^e(\mathbf{g})\exp(-2\pi i\mathbf{g}\cdot\mathbf{r})$$

$$=\left(\frac{|e|}{4\pi^2\varepsilon_0\Omega}\right)\sum_i\frac{[Z-f^x(\mathbf{g})]}{\mathbf{g}^2}\exp(-2\pi i\mathbf{g}\cdot\mathbf{r}). \quad (55)$$

Since we require the value of this expression for $\mathbf{g}=0$, the Debye–Waller factor is neglected. For spherically symmetric atoms, the X-ray scattering factor is

$$f^x(\mathbf{g})=4\pi\int\rho(r)\left(\frac{\sin 2\pi\mathbf{g}r}{2\pi\mathbf{g}r}\right)r^2\,\mathrm{d}r. \quad (56)$$

For V_0, we consider the limiting form of $f^x(\mathbf{g})$ for small $\mathbf{g}$. Expanding $\sin x/x$, we have

$$[Z-f^x(\mathbf{g})]/\mathbf{g}^2=T1,$$

where

$$T1=\mathbf{g}^{-2}[Z-4\pi\textstyle\int\rho(r)r^2\,\mathrm{d}r+(4\pi/3)\times\int\rho(r)r^2(4\pi^2g^2r^2)\,\mathrm{d}r-\ldots].$$

The second term is Z, the number of atomic electrons. Hence,

$$\begin{aligned}T1&=(4\pi^2/3)\textstyle\int\rho(r)r^2(4\pi r^2)\,\mathrm{d}r\\&=(4\pi^2/3)\textstyle\int\rho(r,\theta,\varphi)r^2\,\mathrm{d}\tau\\&=(4\pi^2/3)\textstyle\int\phi r^2\phi^*\,\mathrm{d}\tau\\&=(4\pi^2/3)\langle r^2\rangle,\end{aligned} \quad (57)$$

where ϕ are the wave functions of the atomic orbitals in the rigid-ion approximation. Thus,

$$V_0=\frac{|e|n_0}{3\Omega\varepsilon_0}\langle r^2\rangle=\frac{|e|N\langle r^2\rangle}{3\varepsilon_0}, \quad (58)$$

where n_0 is the number of atoms per cell, N is the number per unit volume and $\langle r^2\rangle$ is the mean-square radius of the atom.

Now the diamagnetic susceptibility per unit volume is, in dimensionless SI units, given by Langevin's

Table 1. *Mean inner potentials V_0 measured by electron diffraction*

Crystal	Method	Result (V)	Reference
Ag	Biprism	20.7	Buhl (1959)
	Biprism	17.0	Keller (1961)
Al	Biprism	13.0	Keller (1961)
	Biprism	12.4	Hoffmann & Jönsson (1965)
	Biprism	11.9	Buhl (1959)
Au	Biprism	21.1	Buhl (1959)
	Biprism	22.1–27.0	Keller (1961)
Be	Biprism	7.8	Jönsson, Hoffmann & Möllenstedt (1965)
Chrysotile	Electron interference	11.5	Yada, Shibata & Hibi (1973)
C	Biprism	7.8	Keller (1961)
Cu	Biprism	23.5	Keller (1961)
	Biprism	20.1	Hoffmann & Jönsson (1965)
GaAs	RHEED	13.2	Yamamoto & Spence (1983)
GaP	RHEED	12.2	Yamamoto & Spence (1983)
Ge	Biprism	15.6	Hoffmann & Jönsson (1965)
MgO	Electron diffraction	13.7	Sturkey (1948)
	Electron diffraction	16	Honjo & Mihama (1954)
	Electron diffraction	15.3	Molière & Niehrs (1955)
	Electron diffraction	13.4	Miyake (1962)
	Electron diffraction	12.3	Tomita & Savelli (1968)
	Electron diffraction	14.0	Yada *et al.* (1973)
Si	Biprism	11.5	Gaukler & Graff (1970)
	Biprism	9.3	Gajdardziska-Josifovska *et al.* (1992)
W	Biprism	23.4	Gaukler & Graff (1970)
ZnS	Biprism	10.2	Buhl (1959)

atomic theory for gases as

$$\chi = -\mu_0 NZe^2/6m\langle r^2\rangle. \quad (59)$$

Hence, we might expect an approximate relationship in diamagnetic crystals of the form

$$\chi = -(\varepsilon_0\mu_0 Z|e|/2m)V_0. \quad (60)$$

This result will not be exact since (59) was derived for gases and because we have represented the crystal as a simple superposition of spherical atoms. An exact relationship can, however, be derived for gases between $f(0)$ and χ (Ibers, 1958). In the old system (first Born approximation) the result is

$$f^B(0) = [4\pi me^2Z/3h^2]\langle r^2\rangle.$$

The first and most extensive comparison of V_0 values (derived from χ) with the values measured by reflection electron diffraction was given by Miyake (1940).

Values of V_0 have been measured by many workers, most commonly by using an electron biprism in an interference experiment. It may also be measured from RHEED experiments (Yamamoto & Spence, 1983). A summary of measurements is given in Table 1. Interferometry measurements provide values of the product V_0t, so the thickness must be known accurately. This problem is avoided in reflection geometry. In transmission work, the highest accuracy has been obtained by using cleaved crystalline wedges, for which the thickness is accurately known at each point (Gajdardziska-Josifovska, McCartney, Weiss, de Ruijter & Smith, 1992). Dynamical corrections, which can introduce errors of more than a volt, were included for the first time in this work.

In conclusion, we see that V_0 has two important interpretations – first as a measure of diamagnetic susceptibility and, secondly [from (57)], as a measure of the 'size' of an atom. It is thus the most sensitive of all the structure factors to the state of ionicity of atoms in a crystal and, because of the terms in r^2 and r^4 in (57), depends strongly on the distribution of outer valence electrons. For example, the simple expression for V_0 in terms of the Gaussian expansion of atomic scattering factors given by Peng & Cowley (1988) might be used. For MgO, this atomic estimate (17.6 V) differs considerably from the experimental value of 13.6 V. The difference is due to the redistribution of charge in the solid state and the sensitivity of (57) provides for this effect. Methods of calculating V_0 in terms of X-ray structure factors are discussed by Becker & Coppens (1990). It is clear that measurements of V_0 by electron diffraction place an important constraint on measured X-ray structure factors through (57) (see Spence & Zuo, 1992, for silicon).

6. Materials index

Table 2 lists many of the accurate structure-factor measurements made by electron diffraction, indexed by material. (An 'accurate' measurement is one with an accuracy in X-ray structure factor of better than 1%.) Care must be exercised in comparing the results of different workers who may use different cell constants, temperatures, units, cell volumes or absorption coefficients for their analysis.

Table 2. *Structure factors measured by electron diffraction*

Crystal	Temperature (K)	Method*	Reference
Ag	293	CV	Fukuhara & Yanagisawa (1969)
	293	CV	Lally *et al.* (1972)
	293	CV	Thomas *et al.* (1974)
Al	293	CV	Lally *et al.* (1972)
	293	CV	Thomas *et al.* (1974)
			Fox, Tabbernor & Fisher (1990)
Al–Li	293	CV	Fox & Fisher (1987)
Au	293	CV	Thomas *et al.* (1974)
Be	293	CV	Fox & Fisher (1988*a*, *b*)
	293	CV	Thomas *et al.* (1974)
Cd		TF	Ichimiya & Uyeda (1977)
	293	CV	Jones (1978)
	293	CV	Fox & Fisher (1988*b*)
CdS		TF	Ichimiya & Uyeda (1977)
α-Co	293	CV	Thomas *et al.* (1974)
	293	CV	Fox & Fisher (1988*b*)
ε-Co	293	CV	Thomas *et al.* (1974)
	293	CV	Fox & Fisher (1988*b*)
Co–Al	293	CV	Fox (1983)
Cr	293	CV	Thomas *et al.* (1974)
	293	CV	Terasaki, Uchida & Watanabe (1975)
Cu	293	CV	Thomas *et al.* (1974)
	293	CV	Rocher & Jouffrey (1972)
	293	CV	Fisher & Shirley (1981)
		CV/CBED	Moodie, Sellar, Imeson & Humphreys (1977)
			Tabbernor, Fox & Fisher (1990)
Cu–Au	293	CV	Fox & Fisher (1986)
			Fox (1984)
αFe	293	CV	Thomas *et al.* (1974)
	293	CV	Terasaki *et al.* (1975)
FeCo	293	CV	Fox (1983)
			Matsuhata *et al.* (1983)
GaAs	RT	CBED	Zuo *et al.* (1988)
			Ishizuka & Taftø (1984)
Ge	293	CV	Hewat & Humphreys (1974)
		Comb.	Shishido & Tanaka (1976)
	293	CV	Matsushita & Kohra (1974)
		CV	Matsumura *et al.* (1989)
Graphite		CBED	Goodman (1976)
Mg	293	CV	Thomas *et al.* (1974)
MgO		Wedge	Herzberg (1971)
		CBED	McMahon in Cowley (1981)
		CBED	Cowley, Goodman & Rees (1957)
		CBED	Molière & Niehrs (1955)
		CBED	Molière & Wagenfeld (1957)
		CBED	Lehmpfuhl & Molière (1961)
		CBED	Uyeda & Nonoyama (1965)
		CBED	Goodman & Lehmpfuhl (1967)
		CBED	Zuo, Foley, O'Keefe & Spence (1989)
Mo	293	CV	Thomas *et al.* (1974)
Nb	293	CV	Thomas *et al.* (1974)
Ni	293	CV	Thomas *et al.* (1974)
NiAl	293	CV	Fox (1985)
			Fox (1983)
			Fox & Tabbernor (1991)
Pt	293	CV	Fox & Fisher (1988*b*)
Si	293	CV	Hewat & Humphreys (1974) (cell X8)
		CBED	Smith & Lehmpfuhl (1975)
		CBED	Terasaki *et al.* (1979)
	293	TF	Kreutle & Meyer-Ehmson (1971)
	293	TF	Ando *et al.* (1974)
	500	TF	Kreutle & Meyer-Ehmson (1969)
Si	293	CV	Thomas *et al.* (1974)
	293	CV	Shishido & Tanaka (1976)
		CBED	Voss *et al.* (1980)
		IKL	Gjønnes & Hoier (1971)
		CV	Matsumura *et al.* (1989)
Ta	293	CV	Thomas *et al.* (1974)
Ti	293	CV	Arii, Uyeda, Terasaki & Watanabe (1973)
V	293	CV	Thomas *et al.* (1974)
	293	CV	Terasaki *et al.* (1975)
W	293	CV	Thomas *et al.* (1974)
Zn	118	CV	Fox & Fisher (1988*a*)
			Jones (1978)
			Tabbernor & Fox (1990)

* CV = critical voltage; Wedge = wedge spot splitting; CBED = convergent-beam electron diffraction; Comb. = combined critical voltage and convergent-beam study; TF = thickness fringes; IKL = intersecting Kikuchi-line method.

7. Discussion, concluding remarks and outlook

The ultimate aim of most of the work in this field has been the study of crystal bonding (Dawson, 1967; Deutsch, 1991; Hewat & Humphreys, 1974; Watenabe *et al.*, 1968; Zuo *et al.*, 1988). For recent reviews of the many attempts to quantify bond types in crystals, see Cohen (1981) and Catlow & Stonehem (1983). For alloys, short-range-order coefficients (Shirley & Fisher, 1979) and composition measurements (Butler, 1972) have also been made, in addition to Debye-temperature measurements (Lally *et al.*, 1972). Structure-factor measurements may also be used to test band-structure calculations (Zuo *et al.*, 1988; Lu & Zunger, 1992). Apart from the physical insight which charge-density maps give into the nature of bonding, these studies have more practical implications; for example, for research into the undesirable low-temperature brittleness of intermetallic alloys used in gas turbines. Since structure-factor measurements may be made from sub-micrometer (or sub-nanometer) sized regions, the problems of defects, dispersion and extinction which arise in X-ray work are avoided. The electron microdiffraction technique may thus be applied to the great variety of metastable microphases which occur in minerals, composite materials and artificial multilayer or quantum-well structures which could not readily be studied by other techniques. The real power of electron-beam methods now lies in their accuracy for structure-factor phase measurement and in their ability to study microcrystals from which large synthetically grown single crystals cannot be grown.

In analyzing CV data, the following sources of error must be considered: (1) off-systematics reflections, if not included in computations; (2) errors in the

absorption potential used (the CV is independent of this for centric crystals in first-order perturbation theory); (3) the influence of anharmonic vibrations (Kuhs, 1988); and (4) errors in the temperature factors used. Errors in the determination of F_X by CV have generally been in the range 0.1-1%. For CBED methods, similar accuracies are obtained. Here errors in accelerating voltage and orientation must be considered. (Thickness and absorption coefficients are treated as refinement parameters.)

The agreement between the X-ray and electron work is difficult to evaluate, since results are frequently quoted at different temperatures, using perhaps different (unstated) cell constants. For Si at 293 K, however, the CV value of $F_X(111)$ is 10.711 (120) compared with the best (averaged) recent experimental X-ray value of 10.6025 (50) (Cummings & Hart, 1988). The original value of Aldred & Hart (1973) obtained by the X-ray *Pendellösung* method (uncorrected for strain, but corrected for nuclear Thomson scattering) was 10.735. In general, both the CV and quantitative CBED methods appear to be more accurate than X-ray powder or single-crystal methods, but less accurate than the X-ray *Pendellösung* method for the cases to which it can be applied.

For conclusions regarding specific materials, the reader is referred to the papers given in Table 2. However, certain general observations recur throughout this work, and these may be classified as referring to semiconductors, elemental metals and alloys.

In the study of bonding in semiconductors, it is important to emphasize the extremely small magnitude of the effects sought. Bonding charge densities in covalent crystals are typically less than 0.01% of the total charge density. The total amount of charge redistributed in the solid state is a small fraction even of the total which falls within the overlap region when neutral-atom charge densities (the promolecule) are placed on the atomic sites of the ideal crystal structure. Thus, most of the charge overlap between atoms is already accounted for by the overlap of neutral atoms, and the additional charge redistribution and resulting total energy reduction which favors the crystalline state is extremely small. Contour maps, if drawn for the total valence charge density using neutral atoms, will be indistinguishable from those for the fully relaxed crystal. Difference (deformation) densities must therefore be plotted and the results from different workers may differ widely, particularly amongst early X-ray results based on kinematic theory, in which difficulties were encountered with extinction and diffuse scattering. The statistical significance of these difference maps are discussed by Maslen (1988) and Dawson (1969). Since the choice of free-atom reference density calculation is somewhat arbitrary, comparisons between difference densities published by different authors for the same crystals are difficult. We suggest, therefore, that reference densities be obtained from the scattering factors in *International Tables for Crystallography* (1989). In this way, comparisons of deformation density can be made between the results of different groups. The pseudoatom fitting procedures of Dawson, Stewart and Coppens should also be used, in which an expansion of the difference density is made in spherical harmonics and Slater orbitals [see Coppens *et al.* (1979) and references therein]. Because of the inevitable presence of noise, temperature effects cannot be completely removed by deconvolution and the measured charge density or potential is therefore a function of temperature. (This makes an important contribution even at 0 K, due to zero-point motion.) The parameter which undergoes the largest change due to bonding, as we have seen, is the mean inner potential V_0.

Silicon has become the model system for all work on semiconductors. In summarizing all work on silicon recently, Deutsch (1991) finds evidence for a 0.5% expansion of the L shell and a breakdown of the rigid-ion approximation used to describe thermal motion. Evidence against the presence of an anharmonic term in the single-atom potential is also found, in agreement with the recent CV measurements of Matsumura *et al.* (1989). A summary of all the measurements consolidated by Cummings & Hart (1988) and a comparison with *ab initio* band-structure computations has recently been given by Lu & Zunger (1992). These researchers find excellent agreement ($R = 0.21\%$) between calculations based on the local density approximation (LDA) and experiment and discuss in detail the important question of the effect of high-order reflections (which are difficult to measure experimentally) on deformation densities. In general, one expects the Fourier coefficients of the deformation density to fall off rapidly with scattering angle, due to the effects of the temperature factor and because core charge is relatively insensitive to bonding. If a suitable (arbitrary) bond volume is defined, it becomes possible to measure the total charge within the bond. Thus, Hewat & Humphreys (1974) found from CV measurements that the total bond-charge redistribution per atom in Si is within 10-20% of that which occurs in Ge. This is consistent with the measured equality of Si-Si and Ge-Ge bond energies, and the assumption that Ge is slightly more electronegative than Si. The 222 reflection in Si is 'forbidden' for spherical atoms, but found experimentally to be about 2% of the magnitude of the 111. It may appear strongly in electron diffraction, allowing its magnitude and sign to be measured with high accuracy [see Ando, Ichimiya & Uyeda (1974) and references therein]. For GaAs, Zuo *et al.* (1988) conclude from quantitative CBED work that the amount of (deformation) charge in the Ga-As bond is 0.071 e,

in good agreement with the results of pseudopotential calculations. Fig. 10 shows their deformation density plotted on the (110) plane which contains the bond. [Some additional structure factors from Bernard & Zunger (1989) have also been included.] Evidence for both ionic and covalent character in the bond is adduced by examining the charge density along the bond.

For the elemental metals (*e.g.* Cu and Al), bonding is found to result from a spherical depletion of charge away from the atomic sites into the spaces between nearest neighbors along ⟨110⟩ (Smart & Humphreys, 1980; Tabbernor, Fox & Fisher, 1990). In these cubic metals it is found that only the 111, 200, 222 and 220 experimental values differ appreciably from the RHF free-atom scattering values. For Cu, Smart & Humphreys (1978) find a peak in the difference potential at the octahedral hole site, thus reducing the depth of the minimum predicted by simple hard-sphere models of atomic packing. Good agreement has been found between CV measurements, X-ray *Pendellösung* measurements and band-structure calculations for Cu by Tabbernor *et al.* (1990). In Be, a build-up of valence electrons is found in the bipyramidal space around the tetrahedral holes (Fox & Fisher, 1988*a*).

For metal alloys, several workers have used the CV technique to measure short-range-order parameters. For example, a two-parameter model which can be used to interpret CVs in substitutional solid solutions is given by Shirley & Fisher (1979), taking into account vibration amplitudes and static displacements (Fox & Shirley, 1983). Indications of covalent bonding in β'-NiAl are given by Fox (1985), based on CV measurements. Bonding is found to result again from a redistribution of electrons from both the Ni and Al sites into the midpoints between nearest-neighbor atoms along [111]. No ionic component of bonding was found (Fox & Tabbernor 1991). A recent comparison of this work with *ab initio* calculations (Lu, Wei & Zunger, 1993) finds good agreement with three of the four measured structure factors, but reports important higher-order terms which contribute a directional *d*-like character to the bonding. They conclude that the bonding is mixed ionic–covalent, with an overall transfer of charge from Al to Ni (relative to neutral atoms).

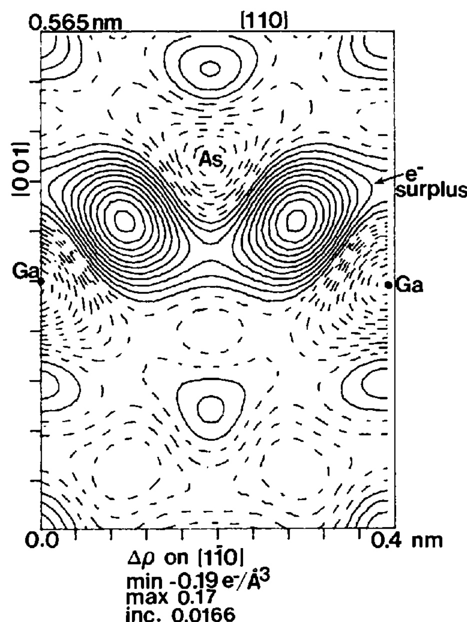

Fig. 10. Charge-density difference map $\Delta\rho(r)$ for GaAs on the (110) plane containing the interatomic bond. Continuous lines are electron-surplus regions [with respect to 'neutral' atoms, defined by structure factors taken from *International Tables for Crystallography* (1989)], dashed lines are electron-deficient regions. The contour increment is 0.0166 Å^{-3}. Difference coefficients included out to 333, some values from Bernard & Zunger (1989).

This work on intermetallic alloys may have important implications for our understanding of mechanical properties. For example, for the case of TiAl, Greenberg, Anisimov, Gornostirev & Taluts (1988) have suggested that low-temperature brittleness in one phase may be due to covalent bonding on the Ti sublattice involving *d* electrons. The Al sublattice is supposed to support metallic bonding involving *s* and *p* electrons. The lattice friction then becomes anisotropic. Dislocations gliding on (111) then see an anomolously deep Peierls valley along [110] directions, along which they may become trapped at low temperature. The thermally activated release of double kinks from these valleys may account for the observed peak in the yield stress.

Experimentally, the field of inorganic electron crystallography is about to enter its most exciting stage. The appearance of imaging energy filters [either of the Omega design (Mayer *et al.*, 1991) or as part of a parallel electron energy-loss spectrometer (Krivanek & Ahn, 1986)], of charge-coupled-device detectors, of field-emission guns for TEM/STEM instruments and of inexpensive RISC work stations and flexible computer control of electron microscopes are certain to revolutionize the field in the near future. For line scans, however, the unrivalled dynamic range of the photomultiplier and serial spectrometer may remain superior. The ability to define a curved trajectory for the filtered scan has proven invaluable for three-beam nonsystematic work. (A fast scan mode is used to display the CBED pattern while defining the locus of the scan required.)

For the future, it would seem that electron crystallography of inorganic crystals is best suited to the study of microcrystals or artificially formed crystals which cannot easily be studied by other methods, to the measurement of structure-factor phases with very high accuracy and to the measurement of the mean inner potential. We have seen that this quantity is more sensitive than any other low-order electron

structure factor to the distribution of bonding electrons (Becker & Coppens, 1990). Since the ideal strength of solids is greatest for crystals consisting of small covalently bonded atoms, a relationship between mechanical properties and V_0 might be sought. The strength of electron scattering makes the study of crystals containing hydrogen possible. In addition, there are many cases for which an X-ray analysis is most productively performed in conjunction with an electron analysis of the same material. Finally, the failure conditions of the local density approximation might be evaluated by comparing measured V_0 and low-order structure factors with calculations for van der Waals bonded crystals, where this approximation is known to be least accurate.

This work was supported by NSF award DMR-9015867 and the facilities of the NSF-ASU Center for High Resolution Electron Microscopy. The author gratefully acknowledges discussions with and contributions from Drs J. M. Zuo, A. Fox, M. O'Keeffe and R. Høier.

Note added in proof: Since this review was submitted, computing speeds have increased considerably. A further speed increase in *REFINE/CB* has been obtained by using the Bethe potential method for weak outer reflections without loss of accuracy (Zuo, 1993).

References

ALDRED, P. J. E. & HART, M. (1973). *Proc. R. Soc. London. Ser. A*, **332**, 239–245.
ALLEN, L. J. & ROSSOUW, C. J. (1989). *Phys. Rev. B*, **39**, 8313–8316.
ANDO, Y., ICHIMIYA, A. & UYEDA, R. (1974). *Acta Cryst.* **A30**, 600–601.
ANGELINI, P. & BENTLEY, J. (1984). *Analytical Electron Microscopy*, edited by D. WILLIAMS & D. JOY, p. 93. San Francisco Press.
ANSTIS, G. (1990). Personal communication.
ARII, T., UYEDA, R., TERASAKI, O. & WATANABE, D. (1973). *Acta Cryst.* **A29**, 295–298.
AVILOV, A. S., SEMILETOV, S. A. & STOROZENKO, V. V. (1989). *Sov. Phys. Crystallogr.* **34**, 110–118.
BECKER, P. & COPPENS, P. (1990). *Acta Cryst.* **A46**, 254–258.
BERNARD, J. E. & ZUNGER, A. (1989). *Phys. Rev. Lett.* **62**, 2328–2331.
BETHE, H. A. (1928). *Ann. Phys. (Leipzig)*, **87**, 55–69.
BEVINGTON, R. (1969). *Data Reduction and Error Analysis for the Physical Sciences.* New York: McGraw-Hill.
BIRD, D. (1990). *Acta Cryst.* **A34**, 208–214.
BIRD, D., JAMES, R. & KING, Q. (1989). *Phys. Rev. Lett.* **63**, 1118–1119.
BIRD, D., JAMES, R. & PRESTON, A. R. (1987). *Phys. Rev. Lett.* **59**, 1216–1218.
BIRD, D. & KING, Q. A. (1990). *Acta Cryst.* **A46**, 202–208.
BIRD, D. M. & JAMES, R. (1988). *Ultramicroscopy*, **26**, 31–38.
BIRD, D. M. & WRIGHT, A. G. (1989). *Acta Cryst.* **A45**, 104–109.
BITHELL, E. G. & STOBBS, W. M. (1989). *J. Microsc.* **153**, 39–47.
BLACKMAN, M. (1939). *Proc. R. Soc. London Ser. A*, **173**, 68–82.
BOE, N. & GJØNNES, K. (1991). *Micron Microsc. Acta*, **22**, 113–114.
BUHL, R. (1959). *Z. Phys.* **155**, 395–402.
BUTLER, E. P. (1972). *Philos. Mag.* **26**, 33–45.
BUXTON, B. & LOVELUCK, J. E. (1977). *J. Phys. C*, **10**, 3941–3955.
BUXTON, B. F. & TREMEWAN, P. T. (1980). *Acta Cryst.* **A36**, 304–315.
CATLOW, C. R. A. & STONEHEM, A. M. (1983). *J. Phys. C*, **16**, 4321–4330.
CHADI, J. (1989). Personal communication.
CHANG, S.-L. (1987). *Crystallogr. Rev.* **1**, 87–149.
COHEN, M. L. (1981). *Structure and Bonding in Crystals.* New York: Academic Press.
COPPENS, P., GURU ROW, T. N., LEUNG, P., STEVENS, E. D., BECKER, P. J. & YANG, Y. W. (1979). *Acta Cryst.* **A35**, 63–72.
COWLEY, J. M. (1953). *Acta Cryst.* **6**, 516–521, 522–529.
COWLEY, J. M. (1967). *Crystal Structure Determination by Electron Diffraction.* In *Progress in Materials Science.* Oxford: Pergamon Press.
COWLEY, J. M. (1981). *Diffraction Physics.* New York: North-Holland.
COWLEY, J. M. (1991). *Ultramicroscopy*, **41**, 335–348.
COWLEY, J. M. (1992). Editor. *Techniques of Transmission Electron Diffraction.* Oxford Univ. Press.
COWLEY, J. M., GOODMAN, P. & REES, A. L. G. (1957). *Acta Cryst.* **10**, 19–25.
CUMMINGS, S. & HART, M. (1988). *Aust. J. Phys.* **41**, 423–433.
DAWSON, B. (1967). *Proc. R. Soc. London Ser. A*, **298**, 379–395.
DAWSON, B. (1969). *Acta Cryst.* **A25**, 12–29.
DEUTSCH, M. (1991). *Phys. Lett.* **A153**, 368–385.
DORSET, D. L. (1983). *Ultramicroscopy*, **12**, 19–32.
DOWNS, J. W., ROSS, F. K. & GIBBS, G. V. (1985). *Acta Cryst.* **B41**, 425–431.
EADES, J. A. (1984). *J. Electron Microsc. Tech.* **1**, 229–241.
FISHER, R. M. & SHIRLEY, C. G. (1981). *J. Met.* (March), pp. 26–33.
FOX, A. G. (1983). *J. Phys. F*, **13**, 1593–1608.
FOX, A. G. (1984). *Philos. Mag.* **50**, 477–489.
FOX, A. G. (1985). *EMAG* 85. *Inst. Phys. Conf. Ser.* No. 78, pp. 379-382. London: Institute of Physics.
FOX, A. G. & FISHER, R. M. (1986). *Philos. Mag.* **A53**, 815–828.
FOX, A. G. & FISHER, R. M. (1987). *Philos. Mag.* **A43**, 260–278.
FOX, A. G. & FISHER, R. M. (1988*a*). *Philos. Mag.* **57**, 197–209.
FOX, A. G. & FISHER, R. M. (1988*b*). *Aust. J. Phys.* **41**, 461–474.
FOX, A. G., O'KEEFE M. A. & TABBERNOR, M. A. (1989). *Acta Cryst.* **A45**, 786–793.
FOX, A. G. & SHIRLEY, C. G. (1983). *J. Phys. F*, **13**, 1581–1595.
FOX, A. G. & TABBERNOR, M. A. (1991). *Acta Metall.* **39**, 669–679.
FOX, A. G., TABBERNOR, M. A. & FISHER, R. M. (1990). *J. Phys. Chem Solids*, **51**, 1323–1339.
FUKAHARA, A. (1966). *J. Phys. Soc. Jpn*, **21**, 2645–2659.
FUKUHARA, A. & YANAGISAWA, A. (1969). *Jpn. J. Appl. Phys.* **8**, 1166–1177.
GAJDARDZISKA-JOSIFOVSKA, M., MCCARTNEY, M., WEISS, J. K., DE RUIJTER, W. & SMITH, D. J. (1992). *Ultramicroscopy.* In the press.
GAUKLER, K. G. & GRAFF, K. (1970). *Z. Phys.* **232**, 190–215.
GJØNNES, J. & HØIER, R. (1971). *Acta Cryst.* **A27**, 313–316.
GJØNNES, K., GJØNNES, J., ZUO, J. & SPENCE, J. C. H. (1988). *Acta Cryst.* **A44**, 810–820.
GOODMAN, P. (1971). *Acta Cryst.* **A27**, 140–147.
GOODMAN, P. (1976). *Acta Cryst.* **A32**, 793–798.
GOODMAN, P. (1978). *Inst. Phys. Conf. Ser.* No. 41, pp. 116–118. London: Institute of Physics.
GOODMAN, P. & JOHNSON, A. W. S. (1977). *Acta Cryst.* **A33**, 997–1001.
GOODMAN, P. & LEHMPFUHL, G. (1967). *Acta Cryst.* **22**, 14–24.
GREENBERG, B., ANISIMOV, V., GORNOSTIREV, Y. & TALUTS, C. (1988). *Scr. Metall.* **22**, 859–869.
HALL, C. R. & HIRSCH, P. B. (1965). *Proc. R. Soc. London Ser. A*, **286**, 158–168.
HALL, S. (1991). *XTAL*. Crystallography Center, Univ. of Western Australia, Nedlands 6009, Australia.
HERZBERG, B. (1971). *Z. Naturforsch.* **26**, 8–17.
HEWAT, E. A. & HUMPHREYS, C. J. (1974). In *High-Voltage Electron Microscopy*, edited by P. SWANN, C. J. HUMPHREYS & M. J. GORINGE. New York: Academic Press.

HIRSCH, P., HOWIE, A., NICHOLSON, R. B., PASHLEY, D. W. & WHELAN, M. J. (1977). *Electron Microscopy of Thin Crystals*. Florida: Krieger.
HOFFMANN, H. & JÖNSSON, C. (1965). *Z. Phys.* **182**, 360-375.
HOHENBERG, P. & KOHN, W. (1964). *Phys. Rev. B*, **136**, 864-878.
HØIER, R. (1972). *Phys. Status Solidi A*, **11**, 597-602.
HØIER, R. & ANDERSSON, B. (1974). *Acta Cryst.* A**30**, 93-95.
HØIER, R., ZUO, J. M., MARTHINSEN, K. & SPENCE, J. C. H. (1988). *Ultramicroscopy*, **26**, 25-39.
HONJO, G. & MIHAMA, K. (1954). *J. Phys. Soc. Jpn*, **9**, 184-199.
HOWIE, A. & VALDRE, U. (1967). *Philos. Mag.* **15**, 777-789.
HUMPHREYS, C. J. (1979). *Rep. Prog. Phys.* **42**, 1825-1887.
HUMPHREYS, C. J. & HIRSCH, P. B. (1968). *Philos. Mag.* **18**, 115-126.
HURLEY, A. & MOODIE, A. F. (1980). *Acta Cryst.* A**36**, 737-738.
IBERS, J. A. (1958). *Acta Cryst.* **11**, 178-183.
ICHIMIYA, A. (1985). *Jpn. J. Appl. Phys.* **24**, 1579-1597.
ICHIMIYA, A. & LEHMPFUHL, G. (1988). *Acta Cryst.* A**44**, 806-809.
ICHIMIYA, A. & UYEDA, R. (1977). *Z. Naturforsch. Teil A*, **32**, 750-764.
International Tables for Crystallography (1989). Vol. A. Dordrecht: Kluwer Academic Publishers.
ISHIZUKA, K. & TAFTØ, J. (1984). *Acta Cryst.* B**40**, 332-337.
JONES, I. P. (1978). *Phys. Status Solidi A*, 47, 385-399.
JÖNSSON, C., HOFFMANN, H. & MÖLLENSTEDT, G. (1965). *Phys. Kondens. Mater.* **3**, 193-207.
KAMBE, K. (1957). *J. Phys. Soc. Jpn*, **12**, 1-26.
KELLER, M. (1961). *Z. Phys.* **164**, 274-288.
KILAAS, R., O'KEEFE, M. A. & KRISHNAN, K. M. (1987). *Ultramicroscopy*, **21**, 47-59.
KOLBY, P. & TAFTØ, J. (1991). *Micron Microsc. Acta*, **22**, 151-164.
KONDO, Y., ITO, T. & HARADA, Y. (1984). *Jpn. J. Appl. Phys.* **23**, L178-L189.
KRAKOW, W. & O'KEEFE, M. (1989). *Computer Simulation of Electron Microscope Diffraction and Images*. New York: The Minerals, Metals and Materials Society.
KREUTLE, M. & MEYER-EHMSON, G. (1969). *Phys. Status Solidi*, **35**, K17-K23.
KREUTLE, M. & MEYER-EHMSON, G. (1971). *Phys. Status Solidi A*, **8**, 111-123.
KRIVANEK, O. L. & AHN, C. (1986). In *Electron Microscopy* 1986, pp. 32-33. Tokyo: Marusen.
KUHS, W. F. (1988). *Aust. J. Phys.* **41**, 369-379.
KURODA, K., TOMOKIYO, Y. & EGUCHI, T. (1981). *Jpn. Inst. Met.* **22**, 535-550.
LALLY, J. S., HUMPHREYS, C. J., METHERELL, A. J. & FISHER, R. M. (1972). *Philos. Mag.* **25**, 321-334.
LEHMPFUHL, G. & MOLIÈRE, K. (1961). *Z. Phys.* **164**, 398-416.
LEWIS, A. L., VILLAGRANA, R. E. & METHERELL, A. J. F. (1978). *Acta Cryst.* A**34**, 138-139.
LIN, Y. P., BIRD, D. M. & VINCENT, R. (1989). *Ultramicroscopy*, **27**, 233-245.
LU, Z. W., WEI, S. H. & ZUNGER, A. (1993). *Acta Met.* Submitted.
LU, Z. W. & ZUNGER, A. (1992). *Acta Cryst.* A**48**, 545-554.
MA, Y., GJØNNES, J. & TAFTØ, J. (1991). *Micron Microsc. Acta*, **22**, 163-164.
MACGILLAVRY, C. H. (1940). *Physica (Utrecht)*, 7, 329-337.
MARTHINSEN, K. & HØIER, R. (1988). *Acta Cryst.* A**44**, 558-562.
MARTHINSEN, K., HØIER, R. & BAKKEN, L. (1990). *Proc. 12th Int. Congr. Electron Microsc.*, pp. 492-493. San Francisco Press.
MARTHINSEN, K., MATSUHATA, H., HØIER, R. & GJØNNES, J. (1988). *Aust. J. Phys.* **41**, 449-463.
MARTHINSEN, M. & HØIER, R. (1989). *Proc. Electron Microsc. Soc. Am.*, edited by G. BAILEY, pp. 484-485. San Francisco Press.
MASLEN, E. N. (1988). *Acta Cryst.* A**44**, 33-37.
MATSUHATA, H. & STEEDS, J. W. (1987). *Philos. Mag.* **55**, 39-55.
MATSUHATA, H., TOMOKIYO, Y., KURODA, K. & EGUCHI, T. (1983). *Jpn. J. Appl. Phys.* **22**, 404-418.
MATSUHATA, H., TOMOKIYO, Y., WATANABE, Y. & EGUCHI, T. (1984). *Acta Cryst.* B**40**, 544-549.
MATSUMURA, S., TOMOKIYO, Y. & OKI, K. (1989). *J. Electron. Microsc. Tech.* **12**, 262-278.
MATSUSHITA, T. & KOHRA, K. (1974). *Phys. Status Solidi A*, **24**, 531-549.
MAYER, J., SPENCE, J. C. H. & MOBUS, G. (1991). *Proc. Electron Microsc. Soc. Am.*, edited by G. BAILEY, pp. 786-787. San Francisco Press.
METHERELL, A. J. F. (1975). *Electron Microscopy and Materials Science. Third Course of the International School of Electron Microscopy*, edited by U. VALDRE & R. REUDL. Commission of the European Communities, Directorate General, Scientific and Technical Information, Luxembourg.
MIYAKE, S. (1940). *Proc. Phys. Math. Soc. Jpn*, **22**, 666-678.
MIYAKE, S. (1962). *J. Phys. Soc. Jpn*, **17**, Suppl. B2, pp. 124-138.
MOLIÈRE, K. & NIEHRS, H. (1955). *Z. Phys.* **140**, 581-599.
MOLIÈRE, K. & WAGENFELD, H. (1957). *Z. Kristallogr.* **110**, 175-192.
MOLLENSTEDT, G. (1989). *Phys. Status Solidi A*, **116**, 13.
MOODIE, A., SELLAR, G., IMESON, D. & HUMPHREYS, C. (1977). Proc. Fifth Int. Conf. on HVEM, Marusen, Kyoto, pp. 33-34.
MOODIE, A. F. (1979). *Chem. Scr.* **14**, 21-38.
NAGATA, F. & FUKUHARA, A. (1967). *Jpn. J. Appl. Phys.* **6**, 1233-1247.
PENG, L. M. & COWLEY, J. M. (1988). *Acta Cryst.* A**44**, 1-5.
PINSKER, Z. G. (1949). *Electron Diffraction*, translated by J. A. SPINK & E. FEIGL. London: Butterworth.
PRESS, W. H., FLANNERY, B., TEUKOLSKY, S. & VETTERLING, W. (1986). *Numerical Recipes*. Cambridge Univ. Press.
RADI, G. (1970). *Acta Cryst.* A**26**, 41-56.
RAIMES, S. (1961). *The Wave Mechanics of Electrons in Metals*. Amsterdam: North Holland.
REIMER, L. (1984). *Transmission Electron Microscopy*. New York: Springer-Verlag.
REZ, P. (1978). D Phil, Univ. of Oxford, England.
REZ, P. (1978). *Acta Cryst.* A**34**, 48-51.
ROCHER, A. M. & JOUFFREY, B. (1972). *Inst. Phys. Conf. Ser.* No. 14, pp. 32-37. London: Institute of Physics.
SELLAR, J., IMESON, D. & HUMPHREYS, C. (1980). *Acta Cryst.* A**36**, 686-696.
SHINOHARA, K. (1932). *Sci. Pap. Inst. Phys. Chem. Res. Tokyo*, **20**, 39-48.
SHIRLEY, C. G. & FISHER, R. M. (1979). *Philos. Mag.* **39**, 91-112.
SHISHIDO, T. & TANAKA, M. (1976). *Phys. Status Solidi A*, **38**, 453-469.
SMART, D. J. & HUMPHREYS, C. J. (1978). *Inst. Phys. Conf. Ser.* No. 41, ch. 3. London: Institute of Physics.
SMART, D. J. & HUMPHREYS, C. J. (1980). *EMAG* 1980, edited by T. MULVEY, pp. 211-223. Bristol: Institute of Physics.
SMITH, P. J. & LEHMPFUHL, G. (1975). *Acta Cryst.* A**31**, S220.
SPACKMAN, M. A. & MASLEN, E. N. (1986). *J. Phys. Chem.* **90**, 2020-2037.
SPEER, S., SPENCE, J. C. H. & IHRIG, E. (1990). *Acta Cryst.* A**46**, 763-772.
SPENCE, J. C. H. (1978). *Scanning Electron Microscopy* 1978, edited by O. JOHARI, pp. 61-73. Chicago: IITRI.
SPENCE, J. C. H. (1992). In *Techniques of Transmission Electron Diffraction*, edited by J. COWLEY. Oxford Univ. Press.
SPENCE, J. C. H. & CARPENTER, R. W. (1986). In *Elements of Analytical Electron Microscopy*, edited by D. JOY, A. ROMIG & H. GOLDSTEIN. New York: Plenum.
SPENCE, J. C. H. & KATZ, M. (1979). Unpublished work.
SPENCE, J. C. H. & ZUO, J. M. (1992). *Electron Microdiffraction*. New York: Plenum.
STEEDS, J. & MANSFIELD, J. (1984). *Convergent Beam Electron Diffraction of Alloy Phases*. Bristol: Adam Hilger.
STURKEY, L. (1948). *Phys. Rev.* **73**, 183-203.
TABBERNOR, M. A. & FOX, A. G. (1990). *Philos. Mag.* **62**, 291-316.
TABBERNOR, M. A., FOX, A. G. & FISHER, R. M. (1990). *Acta Cryst.* A**46**, 165-170.
TAFTØ, J. (1987). *Acta Cryst.* A**43**, 208-211.
TAFTØ, J. & GJØNNES, J. (1985). *Ultramicroscopy*, **17**, 329-339.

TAFTØ, J. & METZGER, T. H. (1985). *J. Appl. Cryst.* **18**, 110-113.
TAFTØ, J. & SPENCE, J. C. H. (1982). *J. Appl. Cryst.* **15**, 60-64.
TANAKA, M. & TERAUCHI, M. (1985). *Convergent-Beam Electron Diffraction.* Tokyo: JEOL Ltd.
TANAKA, M. & TSUDA, K. (1990). Proc. 12th Int. Congr. Electr. Microsc., pp. 518-528.
TERASAKI, O., UCHIDA, Y. & WATANABE, D. (1975). *J. Phys. Soc. Jpn,* **39**, 1277-1301.
TERASAKI, O., WATANABE, D. & GJØNNES, J. (1979). *Acta Cryst.* **A35**, 895-900.
THOMAS, L. E., SHIRLEY, C. J., LALLY, J. S. & FISHER, R. M. (1974). In *High Voltage Electron Microscopy,* edited by P. SWANN, pp. 23-28. New York: Academic Press.
TOMITA, H. & SAVELLI, M. (1968). *C. R. Acad. Sci. Ser. B,* **267**, 580-598.
TOMOKIYO, Y. & KUROIWA, T. (1990). *Proc. 12th Int. Congr. on Electron Microscopy,* pp. 526-527. San Francisco Press.
UNWIN, N. & HENDERSON, R. (1975). *J. Mol. Biol.* **94**, 425-452.
UYEDA, R. (1968). *Acta Cryst.* **A24**, 175-181.
UYEDA, R. & NONOYAMA, M. (1965). *Jpn. J. Appl. Phys.* **4**, 498-509.
VAINSHTEIN, B. (1964). *Structure Analysis by Electron Diffraction.* London: Pergamon.
VALENTINE, R. C. (1966). *Advances in Optical and Electron Microscopy.* New York: Academic Press.
VINCENT, R. & BIRD, D. M. (1986). *Philos. Mag.* **A53**, L35-L46.
VINCENT, R., BIRD, D. M. & STEEDS, J. W. (1984). *Philos. Mag.* **A50**, 765-789.
VINCENT, R., KRAUSE, B. & STEEDS, J. W. (1986). Proc. 11th Int. Congr. Electron Microsc., Marusen, Kyoto, pp. 695-696.
VOSS, R., LEHMPFUHL, G. & SMITH, P. J. (1980). *Z. Naturforsch. Teil A,* **35**, 973-989.
WATENABE, D., UYEDA, R. & KOGISO, M. (1968). *Acta Cryst.* **A24**, 249-250.
WEICKENMEIER, A. & KOHL, H. (1991). *Acta Cryst.* **A47**, 590-597.
WILLIS, B. T. M. & PRYOR, A. W. (1975). *Thermal Vibrations in Crystallography.* Cambridge Univ. Press.
WOLBERG, J. R. (1967). *Prediction Analysis,* p. 60. Princeton: Van Nostrand.
YADA, K., SHIBATA, K. & HIBI, T. (1973). *J. Electron Microsc.* **22**, 223-234.
YAMAMOTO, N. & SPENCE, J. C. H. (1983). *Thin Solid Films,* **104**, 43-56.
YOSHIOKA, H. & KAINUMA, Y. (1962). *J. Phys. Soc. Jpn,* Suppl. B2, pp. 134-149.
ZACHARIASEN, W. (1932). *J. Am. Chem. Soc.* **54**, 3841-3862.
ZUO, J. M. (1992). *Ultramicroscopy,* **41**, 211-227.
ZUO, J. M. (1993). *Acta Cryst.* In the press.
ZUO, J. M., FOLEY, J., O'KEEFE, M. & SPENCE, J. C. H. (1989). *Metal-Ceramic Interfaces.* New York: Pergamon.
ZUO, J. M., GJØNNES, K. & SPENCE, J. C. H. (1989). *J. Electron. Microsc. Tech.* **12**, 29-45.
ZUO, J. M., HØIER, R. & SPENCE, J. C. H. (1989). *Acta Cryst.* **A45**, 839-856.
ZUO, J. M. & SPENCE, J. C. H. (1991). *Ultramicroscopy,* **35**, 185-201.
ZUO, J., SPENCE, J. C., DOWNS, J. & MAYER, J. (1993). *Acta Cryst.* In the press.
ZUO, J. M., SPENCE, J. C. H. & HØIER, R. (1989). *Phys. Rev. Lett.* **62**(5), 547-549.
ZUO, J. M., SPENCE, J. C. H. & O'KEEFFE, M. (1988). *Phys. Rev. Lett.* **61**(3), 353-356.
ZVYAGIN, B. B. (1967). *Electron Diffraction Analysis of Clay Minerals.* New York: Plenum.

Acta Cryst. (1993). **A49**, 260-265

Exact Conditional Distribution of a Three-Phase Invariant in the Space Group *P*1. III. Construction of an Improved Cochran-Like Approximation

BY YAEL POSNER AND URI SHMUELI

School of Chemistry, Tel Aviv University, 69 978 Tel Aviv, Israel

AND GEORGE H. WEISS

Physical Sciences Laboratory, Division of Computer Research and Technology, National Institutes of Health, Bethesda, Maryland 20892, USA

(*Received* 14 *October* 1991; *accepted* 18 *May* 1992)

Abstract

An exact representation of the accurately computable conditional probability density function (c.p.d.f.) of the three-phase invariant for the space group *P*1 was developed in paper I of this series [Shmueli, Rabinovich & Weiss (1989). *Acta Cryst.* **A45**, 361-367]. The computation of this function is too time-consuming for it to be of practical value. It is therefore desirable to find simple approximations based on the exact result that may be more accurate than the familiar Cochran approximation or its extensions. One such approximation, presented here, has the same functional form as the Cochran approximation but with a modified parameter in place of that appearing in Cochran's distribution. Some of the numerical procedures used in the estimation of this modified parameter are also discussed.

Introduction

One of the earliest and still the most frequently employed phase-dependent quantities is the three-phase structure invariant, which is the phase of the

0108-7673/93/020260-06$06.00 © 1993 International Union of Crystallography